

**Aerosol type  
specification in the  
infrared**

L. Clarisse et al.

# A unified approach to aerosol remote sensing and type specification in the infrared

L. Clarisse<sup>1</sup>, P.-F. Coheur<sup>1</sup>, F. Prata<sup>2</sup>, J. Hadji-Lazaro<sup>3</sup>, D. Hurtmans<sup>1</sup>, and C. Clerbaux<sup>3,1</sup>

<sup>1</sup>Spectroscopie de l'Atmosphère, Service de Chimie Quantique et Photophysique, Université Libre de Bruxelles, Brussels, Belgium

<sup>2</sup>Climate and Atmosphere Department, Norwegian Institute for Air Research (NILU) P.O. Box 100, Kjeller, 2027, Norway

<sup>3</sup>UPMC Univ. Paris 6; Université Versailles St.-Quentin, CNRS/INSU, LATMOS-IPSL, Paris, France

Received: 29 August 2012 – Accepted: 4 October 2012 – Published: 11 October 2012

Correspondence to: L. Clarisse (lclariss@ulb.ac.be)

Published by Copernicus Publications on behalf of the European Geosciences Union.

Title Page

Abstract Introduction

Conclusions References

Tables Figures

◀ ▶

◀ ▶

Back Close

Full Screen / Esc

Printer-friendly Version

Interactive Discussion



## Abstract

Atmospheric aerosols impact air quality and global climate. Space based measurements are the best way to observe their spatial and temporal distributions, and can also be used to gain better understanding of their chemical, physical and optical properties. Aerosol composition is the key parameter affecting the refractive index, which determines how much radiation is scattered and absorbed. Composition of aerosols is unfortunately not measured by state of the art satellite remote sounders. Here we use high resolution infrared measurements for aerosol type differentiation, exploiting, in that part of spectrum, the dependency of their refractive index on wavelength. We review existing detection methods and present a unified detection method based on linear discrimination analysis. We demonstrate this method on measurements of the Infrared Atmospheric Sounding Interferometer (IASI) and six different aerosol types, namely volcanic ash, windblown sand, ice crystals, sulfuric acid droplets, ammonium sulfate and smoke particles. The detection of the last three types is unprecedented in the infrared in nadir mode, but is very promising, especially for sulfuric acid droplets which are detected in the lower troposphere and up to 6 months after injection in the upper troposphere/lower stratosphere.

## 1 Introduction

Atmospheric aerosols consist of primary (sea spray, crustal material, smoke, and organic matter) and secondary (sulphates, nitrates, ammonia, volatile organic compounds) components (Kondratyev et al., 2005). Their presence reduces air quality, affecting human health, visibility and life in the whole biosphere (Pöschl, 2005). Aerosols also have an impact on the radiation budget of Earth, causing a net cooling effect on the climate (Forster et al., 2007). The magnitude of the cooling is highly uncertain, but essential for a better understanding of ongoing climate change (Hansen et al., 2011). The reasons for the uncertainty is the large variability in aerosol: on a temporal, spatial

### Aerosol type specification in the infrared

L. Clarisse et al.

Title Page

Abstract

Introduction

Conclusions

References

Tables

Figures



Back

Close

Full Screen / Esc

Printer-friendly Version

Interactive Discussion



and vertical scale and of composition, size, shape, chemical, physical and optical properties (Kaufman et al., 2002; Li et al., 2009). This is in contrast to the greenhouse gas budget which is determined by slow varying long lived gases with definite optical properties. Another element is the great number of different ways in which aerosols can alter the radiative budget of the Earth (Ramanathan et al., 2007). These include direct interactions with solar and terrestrial radiation (Yu et al., 2006) and indirect effects through a multitude of different interaction mechanisms with(in) clouds (Haywood and Boucher, 2000; Li et al., 2011).

Direct effects can be measured, but indirect effects can only be assessed through careful modeling. High temporally and spatially resolved space measurements can greatly help in constraining models. Current dedicated aerosol sounding missions mainly measure the shortwave radiation. Infrared measurements can complement these, offering enhanced sensitivity to coarse mode aerosols; and the possibility of retrieving climatological relevant parameters such as altitude and aerosol composition. Here we focus on the latter.

In the next section we review the state of the art of aerosol detection methods from infrared sounders, which leads up to a unified detection method based on classical discrimination analysis. In Sect. 3 we apply these techniques on measurements of the Infrared Atmospheric Sounding Interferometer (IASI) (Clerbaux et al., 2009; Hilton et al., 2011). IASI is one of the most versatile infrared sounders currently in orbit, designed for both operational and scientific research goals, it has excellent temporal, spatial and spectral coverage and instrumental characteristics. The infrared thermal window is captured from  $645\text{ cm}^{-1}$  to  $2760\text{ cm}^{-1}$  at an apodized spectral resolution of  $0.5\text{ cm}^{-1}$  and low instrumental noise ( $< 0.3\text{ K}$  almost everywhere). We discuss and present results for volcanic ash, windblown sand, ice crystals, sulfuric acid droplets, ammonium sulfate and smoke particles. In Sect. 4 we present our conclusions.

## Aerosol type specification in the infrared

L. Clarisse et al.

Title Page

Abstract

Introduction

Conclusions

References

Tables

Figures

◀

▶

◀

▶

Back

Close

Full Screen / Esc

Printer-friendly Version

Interactive Discussion



## 2 Detection methods

### 2.1 Feature detection

Feature detection methods use elementary (arithmetic) operations on spectral bands or channels to produce detection flags. Such methods have been and are still widely applied on measurements from broadband sounders for the detection of aerosols. The simplest of these is a single threshold on a given band for the detection of thick high altitude clouds. At the other extreme there is, e.g. Ackerman et al. (1998) who published a sophisticated cloud test consisting of 11 different tests on single and pairs of different MODIS bands.

The most commonly used method for aerosol detection is the brightness temperature difference (BTD) between two different spectral bands. Inoue (1985) showed that the difference of the AVHRR bands at 11 and 12  $\mu\text{m}$  is a good indicator for the presence of cirrus clouds. Analogously, Prata (1989) showed a reverse absorption effect between 10 and 11  $\mu\text{m}$  for volcanic ash clouds. These papers also featured the first bispectral diagrams between the BTDs and a reference band. Such graphs can be used to infer quantitative information of two other independent variables such as effective particle radius and optical depth or mass (see Wu, 1987; Parol et al., 1991; Rose et al., 1995 for ice – Wen and Rose, 1994; Yu et al., 2002; Prata and Prata, 2012 for ash). Similar techniques have been applied for detection of windblown sand (Ackerman, 1989) and extended to 3 (Ackerman, 1997; Ellrod et al., 2003; Strabala et al., 1994) or more bands (Pavolonis et al., 2006).

Detection techniques based on BTDs have also been applied on high spectral resolution measurements, e.g. for the detection of ice (Kahn et al., 2003), ash (Carn et al., 2005) and sand (DeSouza-Machado et al., 2006) but also for weak absorbing trace gases, such as sulfur dioxide ( $\text{SO}_2$ ) (Clarisse et al., 2008) and ammonia ( $\text{NH}_3$ ) (Clarisse et al., 2009). The use of BTDs on hyperspectral measurements has the advantage of being able to largely avoid contamination with (other) trace gases. However, by only using a handful of spectral channels they do not fully exploit all the information

## Aerosol type specification in the infrared

L. Clarisse et al.

Title Page

Abstract

Introduction

Conclusions

References

Tables

Figures

◀

▶

◀

▶

Back

Close

Full Screen / Esc

Printer-friendly Version

Interactive Discussion



content captured in such measurements. A full multichannel extension of BTDs for the detection of ash was presented in Gangale et al. (2010) where first and second order polynomials were fitted to high resolution brightness temperature spectra. Detection thresholds could then be introduced on fitted parameters and goodness of fit (see also Newman et al., 2012).

## 2.2 Spectral fitting

Feature detection methods have a physical basis, and can therefore often be used to derive quantitative information. Because of their simplicity they can be employed in operational applications or when large amounts of data need to be processed with limited computational power. In contrast, the most sophisticated methods rely on spectral fitting, where the observed spectrum  $\mathbf{y}$  is matched to a calculated spectrum generated by a forward radiative transfer model  $F_x$  and varying physical parameters  $\mathbf{x}$  (Rodgers, 2000). The physical parameters should include all unknown parameters which influence the forward model in the spectral range of interest.

Spectral fitting is typically ill-conditioned so that the problem needs to be constrained with prior information of the physical parameters  $\mathbf{x}_a$ . Mathematically, the problem is then often formulated as a minimization of the weighted least-squares cost function

$$J = (\mathbf{y} - F_x)^T \mathbf{S}_e^{-1} (\mathbf{y} - F_x) + (\mathbf{x} - \mathbf{x}_a)^T \mathbf{S}_a^{-1} (\mathbf{x} - \mathbf{x}_a). \quad (1)$$

Here the weights are the covariance matrices of the instrumental noise ( $\mathbf{S}_e$ ) and of the prior information ( $\mathbf{S}_a$ ). A common assumption is that of moderate non-linearity of the forward model, in which case the solution  $\hat{\mathbf{x}}$  can be achieved by Newtonian iteration of

$$\mathbf{x}_{i+1} = \mathbf{x}_a + (\mathbf{S}_a^{-1} + \mathbf{K}_i^T \mathbf{S}_e^{-1} \mathbf{K}_i)^{-1} \mathbf{K}_i^T \mathbf{S}_e^{-1} [\mathbf{y} - F_{x_i} + \mathbf{K}_i (\mathbf{x}_i - \mathbf{x}_a)], \quad (2)$$

with covariance

$$\hat{\mathbf{S}}^{-1} = \hat{\mathbf{K}}^T \mathbf{S}_e^{-1} \hat{\mathbf{K}} + \mathbf{S}_a^{-1}. \quad (3)$$

## Aerosol type specification in the infrared

L. Clarisse et al.

Title Page

Abstract

Introduction

Conclusions

References

Tables

Figures

◀

▶

◀

▶

Back

Close

Full Screen / Esc

Printer-friendly Version

Interactive Discussion



## Aerosol type specification in the infrared

L. Clarisse et al.

Title Page

Abstract

Introduction

Conclusions

References

Tables

Figures

◀

▶

◀

▶

Back

Close

Full Screen / Esc

Printer-friendly Version

Interactive Discussion



Here  $\mathbf{K}$  is the Jacobian built up of derivatives  $K_{ij} = \partial F_j(\mathbf{x}) / \partial x_j$ . Under the assumption that both the instrumental noise and prior information can be accurately described as Gaussian probability density functions (pdf), this solution can be shown to be the maximum a posterior solution. Since this solution is the one that maximizes  $P(\mathbf{x}|\mathbf{y})$ , it can be interpreted as the Gaussian probability density function with mean  $\hat{\mathbf{x}}$  and covariance  $\hat{\mathbf{S}}$  and is often referred to as “optimal estimation”.

Note that there are many other (iterative) methods for spectral fitting (Rodgers, 2000), and they are widely employed for the quantitative retrieval of major trace gases (see e.g. Hurtmans et al., 2012). They can also be used to detect weak absorbers, and they are the ultimate way of confirming the presence of their spectral signature in the observed spectrum (see Coheur et al., 2009 and Clarisse et al., 2011 who reported a series of rare trace gas observations from IASI).

A more qualitative way of spectral fitting was introduced in Walker et al. (2011) (see also in this context Rodgers, 2000, p. 70–71 and von Clarmann et al., 2001), who proposed a non-iterative pseudo retrieval of a single physical variable or target species  $\mathbf{x}$  using

$$\hat{\mathbf{x}} = \mathbf{x}_0 + (\mathbf{K}^T \mathbf{S}^{-1} \mathbf{K})^{-1} \mathbf{K}^T \mathbf{S}^{-1} [\mathbf{y} - \mathbf{F}_{\mathbf{x}_0}], \quad (4)$$

where the covariance  $\mathbf{S}$  includes the instrumental noise and the covariance of all physical parameters except  $\mathbf{x}$ . The Jacobian  $\mathbf{K}$  is the derivative of the target species with respect to a fixed average atmosphere. When all constants are omitted, and the column matrix  $\mathbf{K}$  is written as a vector  $\mathbf{k}$ , a quantity

$$R_1 = \mathbf{k}^T \mathbf{S}^{-1} \mathbf{y} = \sum_i \frac{1}{\lambda_i} \mathbf{k}^T \mathbf{v}_i \mathbf{v}_i^T \mathbf{y} \quad (5)$$

is obtained, which can serve as a (non-normalized) measure for  $\mathbf{x}$ . Here  $\mathbf{S} = \sum_i \lambda_i \mathbf{v}_i \mathbf{v}_i^T$  is the eigenvalue decomposition of  $\mathbf{S}$ .

This approach is powerful when  $\mathbf{x}$  is a parameter which does not affect the observed spectrum in a typical atmosphere, as in that case it is straightforward to generate

---

**Aerosol type  
specification in the  
infrared**L. Clarisse et al.

---

[Title Page](#)[Abstract](#)[Introduction](#)[Conclusions](#)[References](#)[Tables](#)[Figures](#)[⏪](#)[⏩](#)[◀](#)[▶](#)[Back](#)[Close](#)[Full Screen / Esc](#)[Printer-friendly Version](#)[Interactive Discussion](#)

a covariance matrix  $\mathbf{S}$  from an ensemble of observed spectra. For instance,  $\text{SO}_2$  is rarely observed with IASI, and the covariance matrix  $\mathbf{S}$  can be generated from randomly observed spectra subject to a simple BTD test on  $\text{SO}_2$ . Not having to retrieve or to model all the other important physical parameters is of great advantage, especially as this method can be applied to large spectral ranges, exploiting the full information content from high resolution sounders. Note that this approach is not equivalent to a full retrieval since (1) it assumes linearity, (2) a fixed Jacobian is used, and (3) it assumes a Gaussian distribution of the probability density function describing the instrumental noise and all other physical parameters. This last condition is valid to some extent, but will fail for outlying features (e.g. rarely observed events such as volcanic eruptions, peculiar surface emissivity effects), causing false detections. With these caveats in mind, the discovery of the pseudo-retrieval method is an important breakthrough in remote sensing and is extremely powerful, in particular for the detection of spectral features spanning a large spectral range.

Spectral fitting approaches have also been applied to the detection and quantification of atmospheric aerosols. The problem is non-trivial and is made more difficult by the intricacies of aerosol radiative transfer which ideally includes the effects of multiple scattering. Another added complexity is the fact that the optical properties of aerosol are never known exactly. These depend on size, shape and composition (e.g. the spectral properties of windblown dust depend largely on their mineral content (Sokolik and Toon, 1999) and can undergo transformations (such as due to particle coagulation) during transport in the atmosphere. This becomes especially important for high spectral resolution measurements. The infinity of different possible aerosol optical properties contrasts with trace gas spectroscopy for which only a limited number of molecular parameters need to be known. In addition to these difficulties, because of spectral interference, trace gases and aerosols should be retrieved simultaneously.

A complete simultaneous fit of trace gas concentrations, aerosol optical depths and effective radii for high resolution IASI spectra was presented in Clarisse et al. (2010a) for scenes with a different dominant aerosol type. It was shown there, that at least

5 different aerosol compositions can be differentiated spectroscopically (ice, biomass burning, sand, volcanic ash and volcanic sulfate). Another recent example of a full fit approach (on selected window channels, and without trace gases) is presented in DeSouza-Machado et al. (2010) for dust retrievals on AIRS spectra.

## 2.3 Distance approaches

An alternative to a full iterative fit is to use of a large amount of precalculated spectra as a lookup table (LUT). Varying parameters can include the target molecule/aerosol loading but also surface temperature, interfering trace gases, aerosol radius, aerosol height and viewing angle. Observed spectra  $\mathbf{y}$  can then be matched to one of the precalculated spectra  $\mathbf{y}_i$  using, e.g. the Euclidean distance, possibly weighted by the instrumental noise covariance matrix  $\mathbf{S}_e$ :

$$J' = (\mathbf{y} - \mathbf{y}_i)^T \mathbf{S}_e^{-1} (\mathbf{y} - \mathbf{y}_i). \quad (6)$$

This distance also appears as the first term in Eq. (1) and is called the Mahalanobis distance (Rencher, 2002). Advantages of LUT approaches are that the obtained solution is guaranteed to be physically meaningful, and that a global minimum can be found of the difference observed-calculated spectra (this is not guaranteed using iterative spectral fit approaches). The LUT approach is especially appealing for the retrieval of aerosols for which the radiative transfer calculations are slow. Examples include retrievals of (cirrus) clouds (Li et al., 2005; Yue and Liou, 2009), dust (Peyridieu et al., 2010 and references therein) and volcanic ash and ice (Gangale et al., 2010; Clarisse et al., 2008; Corradini et al., 2010) from AIRS and IASI. LUT approaches have also been employed for the retrieval of rare trace gases, as in Prata and Bernardo (2007) who proposed a detection algorithm for  $\text{SO}_2$  by looking for a good correlation between precalculated absorbance spectra of  $\text{SO}_2$  and absorbance spectra obtained by dividing observed spectra in a given scene. Their method also used a LUT approach for determining  $\text{SO}_2$  abundances.

## Aerosol type specification in the infrared

L. Clarisse et al.

Title Page

Abstract

Introduction

Conclusions

References

Tables

Figures

◀

▶

◀

▶

Back

Close

Full Screen / Esc

Printer-friendly Version

Interactive Discussion



## Aerosol type specification in the infrared

L. Clarisse et al.

Title Page

Abstract

Introduction

Conclusions

References

Tables

Figures

◀

▶

◀

▶

Back

Close

Full Screen / Esc

Printer-friendly Version

Interactive Discussion



A purely qualitative detection method based on distance was proposed in Clarisse et al. (2010b) for the detection of volcanic ash. Rather than using calculated spectra, a set of real observed spectra was used as a LUT. Observed spectra were then matched against these using the linear Pearson correlation as distance measure. Methods based on auto correlation have also been proposed, both for trace gases (Beer and Norton, 1987) and for clouds (Serio et al., 2000; Masiello et al., 2002).

### 2.4 Methods based on singular value decomposition and principal component analysis

The number of spectral channels in high spectral resolution instruments such as AIRS and IASI far exceeds the number of independent pieces of information contained in them (in a typical observation of a terrestrial atmosphere). Making a principal component analysis (PCA) (Jolliffe, 2002) of an ensemble of spectra is a way of reducing the dimensionality by extracting the principal components of spectral variation and disregarding those that carry no information (Huang and Antonelli, 2001; Antonelli et al., 2004; Klüser et al., 2011). This allows to remove instrumental noise as was illustrated in Atkinson et al. (2010) with a better detection of  $\text{NH}_3$  by the application of a BTD filter on reconstructed spectra.

PCA can also be applied in a different way for the detection of trace gases or aerosols. Principal components should be calculated from a large number of random training spectra to accommodate for all observed variability. However, as discussed in Atkinson et al. (2010), very rare events (volcanic eruptions, large fires) will typically be reconstructed poorly as their weight is too low for their spectral features to be represented in the principal components. This opens up the possibility of using principal components as a detection tool by explicitly avoiding the presence of the target species in the spectra of the training set. This was for instance done for cloud detection in MIPAS observations (Hurley et al., 2009).

In particular, suppose we have a set of clear spectra  $\{s\}$  of length  $n$  (so an ensemble of spectra with no detectable spectral signature due to the presence of the physical

variable or target species  $x$ ). The principal components are the eigenvectors corresponding to the  $m < n$  (to be chosen cleverly) largest eigenvalues of their covariance matrix  $\mathbf{S}$ . Equivalently, they can be obtained from a singular value decomposition of the data matrix consisting of all the clear spectra. The eigenvalue decomposition of  $\mathbf{S}$  can be written as

$$\mathbf{S} = \sum_{i=1}^n \lambda_i \mathbf{v}_i \mathbf{v}_i^T \approx \sum_{i=1}^m \lambda_i \mathbf{v}_i \mathbf{v}_i^T \quad (7)$$

The set  $\{\mathbf{v}_i\}$  form a complete basis of the observation space, so that  $\mathbf{I} = \sum_{i=1}^n \mathbf{v}_i \mathbf{v}_i^T$ . By projecting an arbitrary spectrum onto

$$\mathbf{S}' = \sum_{i=m+1}^n \mathbf{v}_i \mathbf{v}_i^T = \mathbf{I} - \sum_{i=1}^m \mathbf{v}_i \mathbf{v}_i^T, \quad (8)$$

the clear component of the spectrum is disregarded. Doing this on a large number of polluted spectra (these can be simulated or observed but should exhibit a signature due to  $x$ ), we obtain a set of spectra for which again the principal components can be calculated. Projection of an arbitrary observed spectrum  $\mathbf{y}$  onto the vector  $\mathbf{l}$  corresponding to the first principal “polluted” component, then gives a quantitative indication of the presence of the pollutant. This can be written as

$$R_2 = \mathbf{l}^T \mathbf{y} = \mathbf{l}^T \mathbf{S}' \mathbf{y} = \sum_{i=m+1}^n \mathbf{l}^T \mathbf{v}_i \mathbf{v}_i^T \mathbf{y}. \quad (9)$$

Here the notation was chosen to make the relation with Eq. (5) apparent. In Eq. (9) the pollutant vector  $\mathbf{l}$  could be replaced by the Jacobian  $\mathbf{k}$  from Eq. (5) since it is being projected onto the polluted space. Both the pseudo retrieval method and the PCA method project the spectrum on the eigenbasis formed by the covariance matrix of an ensemble of clear spectra. They differ in the applied weights: in Eq. (5) the weights

**Aerosol type specification in the infrared**

L. Clarisse et al.

Title Page

Abstract

Introduction

Conclusions

References

Tables

Figures

◀

▶

◀

▶

Back

Close

Full Screen / Esc

Printer-friendly Version

Interactive Discussion



are  $1/\lambda$ , and thus inversely proportional to the eigenvalues, while in Eq. (9) the weights are 0 (for the largest eigenvalues) and 1 (for the others). So while both methods are clearly related, they will lead to different results. The advantage of the PCA method is that the Jacobian does not need to be known (it can be estimated from the set of polluted observed spectra); while the advantage of the pseudo retrieval method is that it exploits better the full space and does not depend on ad-hoc choices such as the number of principal components.

## 2.5 Use of geophysical information

The detection methods we have discussed until now work on a single spectrum basis. A great deal of information can be extracted by considering ancillary information, in particular observations adjacent in time or space. An example of a detection algorithm which relies heavily on time context is the infrared difference dust index (Legrand et al., 2001; Vergé-Dépré et al., 2006). Here for each location, observations of the past 15 days are taken into account to determine the unpolluted background. The ash correlation method (Clarisse et al., 2010b) takes advantage of spacial context by applying a weaker detection threshold in the neighborhood of certain detections. Another example of an algorithm which explicitly uses spacial context was presented in Watkin et al. (2003), which looks for typical volcanic cloud shapes (e.g. a downwind plume) across infrared images from Meteosat. Similarly, isolated false detections can be avoided by using a median or despeckle filter (Pavolonis and Sieglaff, 2010). Pergola et al. (2004) use a climatology of a region to determine a background of natural variability which may be compared to the signal containing the anomaly (e.g. volcanic ash). The method, termed the Robust AVHRR Technique (RAT), uses statistical measures and is self-adaptive with dynamic thresholds requiring no a priori assumptions. With the increasing use of high temporal and spatial remote sensors, the use of context in detection algorithms should play an increasingly important role.

## Aerosol type specification in the infrared

L. Clarisse et al.

Title Page

Abstract

Introduction

Conclusions

References

Tables

Figures

◀

▶

◀

▶

Back

Close

Full Screen / Esc

Printer-friendly Version

Interactive Discussion



### 3 A general approach

In this section we use basic results of classical discriminant analyses to better understand and generalize some of the detection methods outlined in the previous section. For a complete account of this type of supervised classification we refer to Ripley (1996) and McLachlan (2004). From now on, we assume we deal with the problem of detection of aerosol from high resolution infrared measurements.

#### 3.1 Discriminant analysis

Suppose we have a large training set of observations (here spectra)  $\mathbf{y}$  which can be subdivided in classes or groups based on certain criteria of the observed scene (here aerosol composition). Discrimination analysis is then concerned with the allocation of arbitrary observations to the different classes. For each class  $c$  we can calculate a mean spectrum  $\boldsymbol{\mu}_c$  and covariance matrix  $\mathbf{S}_c$ . If the associated probability density function  $p_c$  is Gaussian and the training set is large enough, then these parameters describe the different classes completely. We denote the prior probability of a randomly chosen observation  $\mathbf{y}$  to be in class  $c$  as  $\pi_c$ . Using Bayes' formula it is straightforward to write down the probability  $p(c|\mathbf{y})$  that  $\mathbf{y}$  belongs to class  $c$ :

$$p(c|\mathbf{y}) = \frac{p(c)p(\mathbf{y}|c)}{p(\mathbf{y})} = \frac{\pi_c p_c(\mathbf{y})}{\sum_d \pi_d p_d(\mathbf{y})} \quad (10)$$

$$= \frac{\pi_c |\mathbf{S}_c|^{-1/2} \exp(-0.5M_c^2(\mathbf{y}))}{\sum_d \pi_d |\mathbf{S}_d|^{-1/2} \exp(-0.5M_d^2(\mathbf{x}))} \quad (11)$$

with

$$M_c(\mathbf{y}) = [(\mathbf{y} - \boldsymbol{\mu}_c)^\top \mathbf{S}_c^{-1} (\mathbf{y} - \boldsymbol{\mu}_c)]^{1/2} \quad (12)$$

the Mahalanobis distance with respect to class  $c$ .

## Aerosol type specification in the infrared

L. Clarisse et al.

Title Page

Abstract

Introduction

Conclusions

References

Tables

Figures

◀

▶

◀

▶

Back

Close

Full Screen / Esc

Printer-friendly Version

Interactive Discussion



Based on this formula we can assign an observation to the class  $c$  with the largest probability  $p(c|\mathbf{y})$ , leading to the so-called Bayesian discrimination. Note that this allocation rule is quadratic in  $\mathbf{y}$  and is therefore also referred to as quadratic discriminant analysis.

This quadratic rule can be simplified under certain assumptions. The prior probabilities are usually not known or hard to determine and are often taken equal  $\pi_c = \pi_d$ . When we also assume that the covariance matrices of the different classes are equal  $\mathbf{S}_c = \mathbf{S}_d = \mathbf{S}$ , then the allocation rule reduces to assigning the observation to the class with smallest Mahalanobis distance. When comparing two different classes, the term  $\mathbf{y}^T \mathbf{S}^{-1} \mathbf{y}$  cancels out and the allocation rule becomes linear in  $\mathbf{y}$ . In particular, for two groups  $c$  and  $p$  we have a linear allocation rule of the form

$$R_3 = \mathbf{m}^T \mathbf{S}^{-1} \mathbf{y} = (\boldsymbol{\mu}_c - \boldsymbol{\mu}_p)^T \mathbf{S}^{-1} \mathbf{y} < \text{constant} \quad (13)$$

While it is easy to write down the analytical expression for this constant, in practice it is usually tuned manually. This two-class discrimination rule also appears as a special case of the so-called Fischer discriminant analysis (or canonical variate analysis). We will not use any of techniques of multiclass discrimination here, but will address the problem indirectly by combining two-class discrimination rules. In particular, we design two-class discrimination rules for each type of aerosol, where in each case the rule attempts to differentiate spectra containing a signature of a specific type of aerosol (polluted spectra  $p$ ) with those that do not (clear spectra  $c$ ).

### 3.2 Interpretation

Equation (13) will only be a good discriminator if the covariance matrix of clear spectra  $\mathbf{S}_c$  and polluted spectra  $\mathbf{S}_p$  are equal to each other. This is fortunately the case for low aerosol loadings (so those that are hardest to detect) as can be seen as follows.  $\mathbf{S}_c$  should be constructed from a representative set of clear spectra not containing a specific type of aerosol. So this covariance matrix will contain the variability and correlation

## Aerosol type specification in the infrared

L. Clarisse et al.

Title Page

Abstract

Introduction

Conclusions

References

Tables

Figures

◀

▶

◀

▶

Back

Close

Full Screen / Esc

Printer-friendly Version

Interactive Discussion



due to all atmospheric parameters affecting the spectrum, except to the specific aerosol type. Now for low aerosol loadings we have  $\mathbf{S}_p \approx \mathbf{S}_c$  as the presence of a thin aerosol layer will affect the spectrum but will not affect the natural variability and correlations due to all other atmospheric parameters. In other words, the pdf of moderately polluted and clear spectra differ only in their mean and not in their covariance. For increasing aerosol loadings the covariance matrix  $\mathbf{S}_p$  will have a component due to aerosol covariance, but no problems are expected here, since these are easier to detect anyway.

The similarities between Eqs. (5) and (13) are no coincidence as they are both derived from maximum likelihood under the assumption of normality. The covariance matrices appearing in both equations can be constructed from clear spectra (in the language of Walker et al. (2011), the ensemble approach). The vector  $\mathbf{m} = \boldsymbol{\mu}_c - \boldsymbol{\mu}_p$  can be interpreted as a Jacobian with respect to a changing aerosol loading. This makes the link with Eq. (5) complete. Note that Eqs. (5) and (13) complement each other. Equation (5) can be used when no large number of polluted training spectra are available, but where the Jacobian is known from laboratory measurements (e.g. for sulfuric acid aerosols). Equation (13) can be used if no representative Jacobians are known, but where numerous training spectra are available (e.g. for volcanic ash), and thus shares this advantage with PCA-type approaches.

### 3.3 Practical considerations

Despite their name, outlying events occur frequently in spectral observations. The pdf of the ensemble of spectra is not Gaussian, and large pollution events or peculiar type of surfaces will in general not be described well in the Gaussian mean and covariance matrix. Such events need to be dealt with when applying the above techniques. The problem can be easily understood with an analogy. Suppose we have a linear discrimination routine to differentiate apples and pears based on a few features (size, weight, color, best matching shape, ...). What will the algorithm do when we present it with an outlier, let us say a banana? Since the observation space is cut in two by the linear discrimination, it will be classified as either an apple or pear based on the Mahalanobis

## Aerosol type specification in the infrared

L. Clarisse et al.

Title Page

Abstract

Introduction

Conclusions

References

Tables

Figures



Back

Close

Full Screen / Esc

Printer-friendly Version

Interactive Discussion



distance; even if that distance is very far from either mean. To avoid such obvious misclassifications, we suggest to combine the linear discrimination approach – which serves as a relative distance measure, with a test based on the absolute distance of an observation to the class mean. In the analogy, it makes common sense to classify a fruit as an apple only if it looks at least a little bit like an apple. As a distance measure we use the Mahalanobis distance with respect to the mean polluted spectra. This is akin to the ash correlation algorithm (Clarisse et al., 2010b), but of course here we want this distance not to serve as the primary criterion for detection, but only to remove some of the false detections.

To have a better grip on the quantities  $R_1$  and  $R_3$ , it is convenient to scale and normalize these properties. We therefore use

$$R_N(\mathbf{y}) = \frac{\mathbf{k}^T \mathbf{S}^{-1} (\mathbf{y} - \boldsymbol{\mu}_c)}{\sqrt{\mathbf{k}^T \mathbf{S}^{-1} \mathbf{k}}}, \quad (14)$$

with  $\mathbf{k}$  the Jacobian or when not available the difference  $\boldsymbol{\mu}_p - \boldsymbol{\mu}_c$ . For clean spectra, this quantity has a mean of zero and a standard deviation of one. This normalization is done implicitly in (Walker et al., 2011) with the use of Z-numbers. Likewise, for the absolute distance we use

$$A_N(\mathbf{y}) = \frac{(\mathbf{y} - \boldsymbol{\mu}_p)^T \mathbf{S}^{-1} (\mathbf{y} - \boldsymbol{\mu}_p)}{N}, \quad (15)$$

with  $N$  so that for clean spectra the mean of  $A_N$  equals one.

Another practical point we need to address is the case where the class of aerosol we wish to detect is insufficiently homogeneous and Gaussian. This is pertinent for mineral aerosol. As noted before, the spectral signature of ash or sand depends largely on the specific mineralogical composition. So while we might want to classify aerosol based on origin (e.g. volcanoes or deserts), their spectral composition might not allow the different possible aerosols signatures to be treated as one aerosol type within the

**Aerosol type specification in the infrared**

L. Clarisse et al.

Title Page

Abstract

Introduction

Conclusions

References

Tables

Figures



Back

Close

Full Screen / Esc

Printer-friendly Version

Interactive Discussion



framework of linear discrimination. For volcanic ash, a global class mean spectrum  $\mu_p$  will contain signatures due to rhyolite but also due to basaltic ash. Such signatures can cancel each other out and the mean spectrum might not correspond to something observable or representative.

5 The problem of inhomogeneity also appeared in Clarisse et al. (2010b) for the selection of an ash reference spectrum. As a solution, not one, but a large number of reference spectra were selected to accommodate for the different spectral signatures. Here we propose a solution along the same lines: instead of trying to detect one type of ash or sand, we divide each category in a number of homogeneous subgroups and  
10 devise detection tests for each of them. But rather than composing these subgroups in an ad-hoc fashion, we use a more systematic approach based on spectral clustering. We have opted here for the  $k$ -means algorithm (Ripley, 1996). It is a method to cluster data in  $k$  groups in such a way that each data point is assigned to the class with smallest distance to its class mean. To start, the algorithm assigns classes randomly, and class means and class assignment are then updated iteratively until convergence.  
15 For the distance metric, we use the Mahalanobis distance (with a covariance matrix calculated from clean spectra). We have applied this spectral clustering both for the detection of ash and sand, with  $k = 10$  as detailed in the next section.

A last practical point is the construction of the clean covariance matrices. For some  
20 of the rarer type of aerosol (e.g. volcanic ash), this is straightforward. For others, such as ice particles/cirrus clouds, a prior detection method is required to filter out polluted spectra. Here we used mainly BTM type methods. Also, rather than using a single covariance matrix, we can increase sensitivity by making use of several covariances for different time/space intervals. For example volcanic ash detection over the South  
25 Pacific ocean should be easier than detection over the Saharan desert. The typical covariance over these different regions is clearly different and this can be exploited by the use of a different covariance matrix. In next section, depending on the specific aerosol type, we will make use of different covariance matrices for observations over

## Aerosol type specification in the infrared

L. Clarisse et al.

Title Page

Abstract

Introduction

Conclusions

References

Tables

Figures

◀

▶

◀

▶

Back

Close

Full Screen / Esc

Printer-friendly Version

Interactive Discussion



ocean or land, for observations contained in different latitude–longitude grid boxes or for different periods of the year.

## 4 Applications

In this section we present examples of the different types of aerosol that we were able to distinguish with IASI. Note that for the analysis we only use a subset of IASI channels, namely 100 window channels between  $750\text{ cm}^{-1}$  and  $1250\text{ cm}^{-1}$  in brightness temperature space. Channel selection is a constraint based on a priori knowledge of the window channels. While the above methods can clearly utilize the full spectrum, using only a subset of channels is resource-friendly and allows for efficient storage and reprocessing of large time periods of IASI data. Using the full spectrum should lead to slightly better results, although we expect that these 100 channels capture the majority of the aerosol information content. In the examples below, the goal is not to present an ultimate or finished detection product, but rather to demonstrate the huge and largely unexplored possibilities of infrared instruments for aerosol type specification. Where applicable, Jacobians were calculated for a standard atmosphere (NOAA-NASA-USAF, 1976), with infrared spectra simulated using an advanced radiative transfer forward model (Clarisse et al., 2010a) with optical properties of aerosol calculated with Mie theory.

### 4.1 Ice crystals

The most common observations of ice crystals are in high altitude cirrus clouds (Lynch et al., 2002). Also volcanic ice is regularly observed in eruptive volcanic plumes (Rose et al., 2004). Cirrus clouds play an important role in the global climate and have a large contribution on the radiative budget, because they interact with both terrestrial and solar radiation. Detection from space has been accomplished using a variety of different instruments, e.g. AVHRR (Inoue, 1985; Parol et al., 1991), HIRS (Wylie et al., 1994;

## Aerosol type specification in the infrared

L. Clarisse et al.

Title Page

Abstract

Introduction

Conclusions

References

Tables

Figures

◀

▶

◀

▶

Back

Close

Full Screen / Esc

Printer-friendly Version

Interactive Discussion



Stubenrauch et al., 2006), MLS (Wu et al., 2008), MISR (Prasad and Davies, 2012), Cloudsat/CALIPSO (Haladay and Stephens, 2009; Sassen et al., 2008), MODIS (Mace et al., 2005) and AIRS (Kahn et al., 2003; Li et al., 2005).

The infrared window 750 to 1250  $\text{cm}^{-1}$  is very sensitive to clouds. Water clouds absorb almost uniformly over this spectral range and will cause a drop in the observed baseline. Thicker clouds can become opaque and will absorb most of all of the incoming radiation whilst emitting radiation corresponding to its cloud top temperature. Ice clouds on the other hand have a very characteristic decreasing infrared absorption signature between 700 and 1000  $\text{cm}^{-1}$  (Smith et al., 1998) caused by the optical properties of ice crystals. The exact feature will depend largely on the size distribution of the ice crystals but is most pronounced for smaller ice particles ( $< 10 \mu\text{m}$ ) and moderate optical depths (semi-transparent optical thicknesses) (Kahn et al., 2003).

For the calculation of a Jacobian, a gamma size distribution was assumed, with an effective radius of 10  $\mu\text{m}$  (Clarisse et al., 2010a) and refractive indices were taken from Warren and Brandt (2008). One global clean (unpolluted) covariance matrix was constructed from 30 days in 2009. Ideally, all spectra with signatures due to ice particles should be removed. Here, we excluded spectra with an obvious cirrus signature; i.e. with a brightness temperature difference of the channels at 1231.5  $\text{cm}^{-1}$  and 874.75  $\text{cm}^{-1}$  superior to 5 K.

As an example of cirrus detection, we plot in Fig. 1 the quantity  $R_N$  over Middle America on 15 September 2010. Also shown in grays is the EUMETSAT Level 2 cloud coverage product (August et al., 2012). Typical tropical cirrus (Wang and Dessler, 2012) can be observed over South America, with clear detection especially over the parts with a low percentage of cloud coverage. Hurricane Igor can be seen over the Atlantic Ocean with characteristic cirrus fanning away from its center. It is clear from this example that the presented cirrus detection works best for semi-transparent cirrus clouds. Note that optically thick clouds have a flat absorption feature and are almost indistinguishable from thick cirrus clouds in the infrared.

## Aerosol type specification in the infrared

L. Clarisse et al.

Title Page

Abstract

Introduction

Conclusions

References

Tables

Figures

◀

▶

◀

▶

Back

Close

Full Screen / Esc

Printer-friendly Version

Interactive Discussion



## 4.2 Sulfuric acid droplets

Oxidation of SO<sub>2</sub> produces sulfuric acid, which leads to the formation of sulfate aerosol and in particular sulfuric acid–water solution drops (Steele and Hamill, 1981; Turco et al., 1982; Hamill et al., 1982). Here, our main focus is on upper tropospheric and stratospheric sulfuric acid droplets which are formed within hours to weeks after injection of SO<sub>2</sub> gas and have an atmospheric lifetime of months to years. A direct effect of sulfuric acid aerosols is their interaction with radiation, i.e. scattering of shortwave radiation and absorption of longwave radiation (Stenchikov et al., 1998). In general, large stratospheric injections of sulfuric acid aerosols lead to both a local atmospheric warming and a global cooling of the climate (Robock, 2000). Very large injections can have a dramatic effect on air quality and human health (Schmidt et al., 2011). Sulfuric acid aerosols also have a detrimental effect on aircrafts, potentially causing damage to the windshield, turbine, engine and airframe (Carn et al., 2009).

In the satellite era there have been several large volcanic stratospheric SO<sub>2</sub> injections, most notably due to the eruptions of El Chichón in 1982 and Mount Pinatubo and Cerro Hudson in 1991. A couple of instruments were long enough in orbit to measure the associated increase and decrease in aerosol loading. Examples include the limb viewing SAGE II instrument at visible and near infrared wavelengths (Thomason et al., 1997; Bauman et al., 2003) and CLAES and ISAMS at infrared wavelengths (Rogers et al., 1998; Lamberta et al., 1997). While shortwave instruments can measure an increase in aerosols, infrared instruments are sensitive to particle composition and in ISAMS infrared measurements performed after the Pinatubo eruption, it was possible to unambiguously identify the specific infrared spectral signature of sulfuric acid–water drops (Grainer et al., 1993; Echle et al., 1998). Nadir observations of sulfuric acid aerosols include the optical depth measurements made by the NOAA/AVHRR sounder (Stowe et al., 1992; Long and Stowe, 1994) and infrared HIRS observations (Ackerman and Strabala, 1994). More recently, sulfuric acid observations from the moderate (1–2 Tg SO<sub>2</sub>) eruptions of Kasatochi and Sarychev were reported using the CALIPSO

### Aerosol type specification in the infrared

L. Clarisse et al.

Title Page

Abstract

Introduction

Conclusions

References

Tables

Figures



Back

Close

Full Screen / Esc

Printer-friendly Version

Interactive Discussion



lidar, OSIRIS limb sounder and ACE occultation measurements (Kravitz et al., 2011; Doeringer et al., 2012; O'Neill et al., 2012; Haywood et al., 2010; Bourassa et al., 2010; Vernier et al., 2011). Example IASI spectra of sulfuric acid aerosol observations were shown in Karagulian et al. (2010), Clarisse et al. (2010a) and Haywood et al. (2010).

5 In the current detection framework, a clean covariance matrix can be built from time periods which are assumed to be relatively clear of enhanced concentrations of sulfuric acid aerosol. In particular, we used a complete year of IASI observations: April and May 2009 and 2010 for the other months (because of the Eyjafjallajökull eruptions in April and May 2010). Taking such a large time period and so many days minimizes  
10 the influence of smaller and short lasting volcanic eruptions. To increase sensitivity, not a global but a local covariance matrix was built, representative for each 10 by 10 degree grid cell. For the calculation of the Jacobian, a choice has to be made for a representative size distribution, temperature and sulfate concentration (Steele and Hamill, 1981; Grainer et al., 1993). A concentration of 75 % H<sub>2</sub>SO<sub>4</sub> was chosen, with droplets  
15 following a logarithmic size distribution with an effective radius of 1 μm. Refractive indices were taken from Tisdale et al. (1998) at a temperature of 215 K (representative for the Kasatochi and Sarychev injection altitudes).

The spectral signature of sulfuric acid aerosols in the region 750–1250 cm<sup>-1</sup> is a wavy pattern, caused by several absorption bands, but with largest absorption for wavenumbers above 1100 cm<sup>-1</sup> (Boer et al., 2007; Clarisse et al., 2010a; Echle et al.,  
20 1998). Since we expect sulfuric acid aerosols in volcanic plumes we must be careful for potential spectral interference with SO<sub>2</sub>, which has the ν<sub>1</sub> absorption band around 1152 cm<sup>-1</sup> (Flaud et al., 2009). It is not the strongest absorption band, but definitely large enough to cause interference, especially since volcanic plumes were omitted in  
25 the calculation of the clean covariance matrix. To avoid any possible interference, we treat spectra with a detectable SO<sub>2</sub> signature separately. As a measure of the signature we use the SO<sub>2</sub> BTD used in Clarisse et al. (2012). It flags on the ν<sub>3</sub> band, which is about an order of magnitude stronger than the ν<sub>1</sub> absorption band. We have treated all spectra with a BTD larger than 0.75 K separately, as this puts the corresponding

## Aerosol type specification in the infrared

L. Clarisse et al.

[Title Page](#)[Abstract](#)[Introduction](#)[Conclusions](#)[References](#)[Tables](#)[Figures](#)[⏪](#)[⏩](#)[◀](#)[▶](#)[Back](#)[Close](#)[Full Screen / Esc](#)[Printer-friendly Version](#)[Interactive Discussion](#)

variations in the  $\nu_1$  absorption band for the other spectra well below the instrumental noise. For affected spectra, we make use of separate Jacobian and covariance matrices, excluding the spectral region  $1152 \pm 65 \text{ cm}^{-1}$ . Volcanic ash and other rare events can also cause interferences, but such spectra are easily excluded using the absolute distance – Eq. (15). We conservatively filtered out observations with an absolute distance exceeding one.

The results for 3 yr of IASI observations in the Northern Hemisphere are shown in Figs. 2 and 3. Figure 2 shows  $\text{SO}_2$  BTD (negative values indicative for  $\text{SO}_2$ ) and  $R_N(\text{H}_2\text{SO}_4)$  following the eruption of Sarychev on 12 June 2009, after 0, 7, 14, 30 and 90 days. From the very onset,  $\text{H}_2\text{SO}_4$  is detected and follows nicely the  $\text{SO}_2$  distribution. Already after two weeks, the  $\text{H}_2\text{SO}_4$  detection exceeds the  $\text{SO}_2$  detection. After 30 days sulfuric acid aerosol is detected everywhere north of  $40^\circ \text{ N}$  and it continues to be detectable for many more months after the eruption.

Figure 3 shows the Northern Hemisphere minimum daily value  $\text{SO}_2$  DBT and average value of  $R_N(\text{H}_2\text{SO}_4)$ . Both the Kasatochi and Sarychev eruption had a clear long term impact on sulfuric acid concentrations in the Northern Hemisphere. Although the total  $\text{SO}_2$  injection from Kasatochi ( $> 1.5 \text{ Tg}$ ) was larger than of Sarychev ( $\approx 1 \text{ Tg}$ ) (Krotkov et al., 2010; Clarisse et al., 2012), it seems that the lifetime of the sulfuric acid aerosol from Sarychev was the largest. This is consistent with observations from the OSIRIS limb sounder which found a larger maximum mean aerosol optical depth from Sarychev (Haywood et al., 2010; Bourassa et al., 2012). A similar observation can be made from sulfuric acid aerosol retrievals from ACE (Doeringer, 2011; Doeringer et al., 2012). In the absence of large injections, as was the case in 2010, there is some fluctuation in the mean value of  $R_N(\text{H}_2\text{SO}_4)$  and looking at the inter-annual variability on Fig. 3 there is also a recurring seasonal minimum between February and June, possibly related to ozone seasonality. Although we have not tried this here, it is likely that this seasonality would disappear when making use of dedicated seasonal covariance matrices.

## Aerosol type specification in the infrared

L. Clarisse et al.

[Title Page](#)[Abstract](#)[Introduction](#)[Conclusions](#)[References](#)[Tables](#)[Figures](#)[⏪](#)[⏩](#)[◀](#)[▶](#)[Back](#)[Close](#)[Full Screen / Esc](#)[Printer-friendly Version](#)[Interactive Discussion](#)

**Aerosol type  
specification in the  
infrared**

L. Clarisse et al.

Title Page

Abstract

Introduction

Conclusions

References

Tables

Figures

◀

▶

◀

▶

Back

Close

Full Screen / Esc

Printer-friendly Version

Interactive Discussion



The previous examples focus on the larger eruptions of 2008 and 2009, but  $\text{H}_2\text{SO}_4$  can also be detected in smaller eruptions or sustained degassing. Examples of the latter are presented in Fig. 4 which shows monthly averaged maps of  $R_N(\text{H}_2\text{SO}_4)$  for three volcanoes. The two panels on the left show a large plume over Central Africa originating from the Nyamuragira volcano. It is Africa's most active volcano and one of the largest recent natural sources of  $\text{SO}_2$  emissions (Carn and Bluth, 2003; Bluth and Carn, 2008). On 6 November 2011 the Nyamuragira volcano violently erupted and continued to do so for 5 months. Injection altitudes were between 4–8 km (Theys et al., 2012). Throughout November,  $\text{SO}_2$  can be detected in the vicinity of the volcano and drifting westwards. The November monthly mean shows  $\text{SO}_2$  mainly over the D.R. of Congo (see also the monthly mean from OMI shown in inset).  $\text{H}_2\text{SO}_4$  detection extends thousands of kilometers, well over the South Atlantic with a maximum detection at some distance away from the emitting source (1000–2000 km). This is consistent with a lifetime of  $\text{SO}_2$  of the order of one day (Bluth and Carn, 2008), wind velocities of the order of 500 km per day ( $\sim 6 \text{ ms}^{-1}$ ) and the fact that sulfuric acid aerosols that have undergone some growth or coagulation are easier to detect. The top right panel of Fig. 4 shows the August 2008  $\text{H}_2\text{SO}_4$  plume from Kilauea (Hawaii). The plume has a maximum close to the volcano and another 1500–2500 km downwind. The detection is remarkable as the injection height of the relatively mild eruptions at Kilauea is low. In fact, almost no  $\text{SO}_2$  is measured using the BTD-based IASI  $\text{SO}_2$  retrieval (Clarisse et al., 2012) which uses spectral channels with a penetration depth between 3 and 6 km. Similarly, a  $\text{H}_2\text{SO}_4$  signal was picked up near the Galápagos Islands in April 2009 for which no coincident  $\text{SO}_2$  was measured with IASI. The plume depicted in the lower right corner of Fig. 4, can be attributed to activity of the Fernandina volcano.

**4.3 Windblown sand**

Sand, dust and other soil derived aerosol is emitted directly rather than formed in the atmosphere. As one of the most abundant types of aerosol it has a multitude of climatological and environmental impacts (Gassó et al., 2010). Sand interacts with a wide

range of radiation and is readily sensed by most aerosol sensors, see e.g. Carboni et al. (2012) for a comparison of AOD of Saharan dust from eight different instruments. Retrievals over land, and especially deserts is challenging in the thermal infrared because of variable surface emissivity and in the solar spectral range because of high reflectivity. Thermal infrared instruments are very sensitive to sand aerosols, and they have the advantage of being able to distinguish them from other aerosol types. They can also be used to retrieve effective radius and height (Pierangelo et al., 2004, 2005; Peyridieu et al., 2010; DeSouza-Machado et al., 2010).

As explained above, to deal with the large variety of different sand signatures, we have constructed 10 polluted class mean spectra  $\mu_p$  using the  $k$ -means algorithm. Twelve sand/dust storm scenes were selected directly over, and transported from the Sahara, Gobi, Arabian and Simpson deserts both during night and day. Effort was made to confirm the presence of sand aerosols using either visible (MODIS) or lidar (CALIPSO) imagery. From these different scenes, sand polluted spectra were selected based on DBT tests and fed to the  $k$ -means algorithm. The 10 resulting class mean spectra are shown in Fig. 5. The observed large variability in the spectral signatures supports the choice to work with different classes, although the number of classes could probably be reduced. For most class means, the characteristic V-shape between 800 and 1200  $\text{cm}^{-1}$  is obvious. This shape is due to the presence of Si-O fundamentals in minerals such as quartz, illite and montmorillonite (Hunt, 1982; Clark, 1999; Sokolik and Toon, 1999). Other tentative assignments of calcite and kaolinite have also been indicated.

The problem of constructing a clean covariance matrix is not trivial, and here we have opted for a recursive approach as a better sand detection allows constructing a better covariance matrix. First, to better accommodate for surface emissivity effects for the detection of windblown sand we treat land and ocean separately. In the first iteration, a sand detection test was designed based on a single relative distance  $R_N$ . Here, the clean covariance matrices (one for land and one for ocean) were constructed from all spectra of one day (so also contaminated spectra) and the polluted class mean from

## Aerosol type specification in the infrared

L. Clarisse et al.

[Title Page](#)[Abstract](#)[Introduction](#)[Conclusions](#)[References](#)[Tables](#)[Figures](#)[⏪](#)[⏩](#)[◀](#)[▶](#)[Back](#)[Close](#)[Full Screen / Esc](#)[Printer-friendly Version](#)[Interactive Discussion](#)

the mean of the twelve dust scenes described above. Detection in this way is noisy, but allows to filter out the most obvious dust scenes. In the second iteration, this basic test was used to design better clean covariance matrices from 24 days of spectra. These matrices were used to replace the covariance matrices in the first test to obtain a better detection test. This second detection test was then used to construct the final clean covariance matrices.

Using these, and the 10 different class means, 10 different sand detection tests were designed, each using the value of  $R_N$  as primary detection criterion and  $A_N$  to remove false alerts. The corresponding detection thresholds were manually tuned. The result for a day in March and one in April are shown in Fig. 6. The colors refer to the individual tests, but in case of detection by multiple tests, only the color corresponding to the first successful detection is indicated. The March plot (top panel) shows large synoptical scale transport patterns westwards from the Saharan desert and eastwards from the Taklamakan and Gobi desert. Looking at North Africa and the land/ocean transitions it is clear that detection over land is almost as good as over ocean for these large plumes. The April plot (bottom panel) depicts a very large plume of Saharan dust being transported towards the UK and the rest of Europe. The plume originated from the North African coast on 5 April and was transported over the Atlantic and Spain reaching the UK, Norway and Sweden on 8–10 April and reaching back to Saudi-Arabia on the 13th. Note that most of the sand is detected with tests 2, 4, 7 and 8. This has to do with parameter tuning but also with the fact that some signatures only manifest themselves in special thermal conditions. An example is test 1 which is observed very close to the west coast of Africa in the bottom panel and seems to occur when there is almost no or negative thermal contrast between the dust plume and the underlying ocean.

Resulting monthly averages of detected sand are shown in Fig. 7 for the months January and June 2011. The figure was obtained by gridding the daily detection maps and calculating the percentage of detected sand spectra in each grid cell. The plots were saturated at 20%. For the moment there does not exist a global satellite derived sand/dust product to compare these plots with. A qualitative comparison with AIRS

## Aerosol type specification in the infrared

L. Clarisse et al.

Title Page

Abstract

Introduction

Conclusions

References

Tables

Figures



Back

Close

Full Screen / Esc

Printer-friendly Version

Interactive Discussion



optical depths (Peyridieu et al., 2010) over the Atlantic ocean and Arabian sea shows however an excellent correspondence. Detection over land is more difficult than over ocean; especially for lower loadings (e.g. in January). The false alert rate is in general low (smaller than 1 % globally, larger in the tropics) except in specific locations marked by peculiar surface emissivity features (e.g. over Lake Eyre, Australia). Almost no interference with other aerosol types is found, except with ash, which will be dealt with in next section.

#### 4.4 Volcanic ash

Volcanic ash generally refers to small (less than 2 mm) pulverised particles of pieces of volcanic glass and rock. Their atmospheric lifetime range from minutes to months depending on injection height and particle size (Rose and Durant, 2009). The main motivation for routine monitoring of fine volcanic ash from space is mitigation of the safety threat it poses to aviation. Volcanic ash causes erosion and abrasion to the aircraft (e.g. to the windscreen) and readily melts inside the engine, potentially leading to engine failure (see Casadevall (1994); Miller and Casadevall (2000); OFCM (2004) and references therein). Currently a global network of nine volcanic ash advisory centers (VAACs) reports ash observations and forecasts. These rely on transport and dispersion models fed by ground-based data (lidar/radar), satellite observations and reports from pilots. Until April 2010 the emphasis of the volcanic ash problem was on the safety aspect. However, during and after the April–May eruption of Eyjafjallajökull eruption in 2010, a lot of attention was given to the financial aspect. Indeed the cost of rerouting or canceling flights can be very large, e.g. for the period of 15 to 21 April 2010, airlines lost at least US \$1.7 billion in revenue (Mazzocchi et al., 2010). The eruptions of Eyjafjallajökull in 2010 and Grímsvötn reinforced the need for, and importance of accurate high spatial and temporal ash measurements and modeling forecasts (Stohl et al., 2011; Zehner, 2012).

The infrared spectral range is just like for windblown dust, the preferred way of differentially observing volcanic ash. For a review of different techniques and instruments

### Aerosol type specification in the infrared

L. Clarisse et al.

Title Page

Abstract

Introduction

Conclusions

References

Tables

Figures

◀

▶

◀

▶

Back

Close

Full Screen / Esc

Printer-friendly Version

Interactive Discussion



see Prata (2009). Traditionally broadband instruments have been used for the detection of volcanic ash and their general small footprint and high revisit time remain a decisive advantage (Pavolonis and Sieglaff, 2010; Prata and Prata, 2012). Only a few papers deal with ash measurements from high spectral resolution instruments, and these report better sensitivity to thin plumes and better differentiation of ash with other atmospheric parameters (clouds, water vapor, sand and surface emissivity features) (Gangale et al., 2010; Clarisse et al., 2010b; Klüser et al., 2012).

In the current framework, as volcanic ash is only sporadically observed, it is easy to generate the covariance matrices. For simplicity, we have used the same ones as for the detection of sulfuric acid aerosols. The same distinction was also made for spectra with and without a detectable SO<sub>2</sub> signature. So, to avoid cross contamination, a reduced spectral signature is used in case of positive SO<sub>2</sub> detection. There is no unique spectral signature of ash because of variable composition and size distribution. For the calculation of the polluted class mean(s) we have adopted therefore the same approach as for sand, selecting spectra of ten different ash scenes from eruptions of Eyjafjallajökull, Grímsvötn, Puyehue-Cordón Caulle, Soufrière Hills, Shiveluch and Sarychev. These spectra were then clustered using the *k*-means algorithm for which class means are shown in Fig. 5. The algorithm separates the different eruptive plumes remarkably well and the different classes clearly exhibit a difference in composition but also in magnitude. Most striking is the difference around 860 cm<sup>-1</sup> (830 to 900 cm<sup>-1</sup>) going from concave for felsic ashes (e.g. from Puyehue-Cordón Caulle) to convex for mafic ashes (Grímsvötn). The concavity of felsic ashes was noted in Gangale et al. (2010) in spectra of the rhyolitic ash of Chaitén and is only partially reproduced in the widely used refractive measurements of Pollack et al. (1973) which has the concave peak closer to 800 cm<sup>-1</sup>. See in this context also Newman et al. (2012) for example plots of high resolution spectral fits of rhyolitic and basaltic volcanic ash.

In the same way as was done for sand, detection threshold were manually tuned. While the use of different covariance matrices in different latitude/longitude gridboxes already guarantees few false detections due to sand and surface emissivity features, an

## Aerosol type specification in the infrared

L. Clarisse et al.

Title Page

Abstract

Introduction

Conclusions

References

Tables

Figures

◀

▶

◀

▶

Back

Close

Full Screen / Esc

Printer-friendly Version

Interactive Discussion





and may be found in either solid or aqueous form, and can be pure, mixed with other secondary aerosol or coated on primary aerosol (Wang et al., 2008; Yu et al., 2012; Zhang et al., 2007). They represent a major part of anthropogenic aerosol, affecting air quality and impacting significantly the radiative budget (Adams et al., 1999; Martin et al., 2004). To our knowledge remote sensing measurements of ammonium sulfates have not been reported until now.

It is however well known that ammonium sulfate has a strong absorption band near  $1115\text{ cm}^{-1}$  (see Fig. 8), which is favorably located in the atmospheric window. Refractive indices of ammonium sulfate have been measured since the 1970's both in crystalline (Volz, 1973; Toon et al., 1976; Earle et al., 2006; Segal-Rosenheimer et al., 2009) and aqueous form (Remsberg, 1973; Downing et al., 1977; Boer et al., 2007). For the calculation of the Jacobian, we use the recent publicly available dataset from Earle et al. (2006) assuming a logarithmic size distribution with an effective radius of  $0.2\ \mu\text{m}$ . Because we expect ammonium sulfate aerosols close to the surface, for this type of aerosol we only used cloud filtered spectra. Covariance matrices were constructed separately for land and ocean on global data of 24 days covering all months. As we have a priori no easy way of filtering out spectra with an ammonium sulfate signature, the idea of using a global covariance matrix is to reduce the weight of such spectra.

Ammonium sulfate was unambiguously identified over East China for May–July 2010, see Fig. 9; and confirmed by visual inspection of observed spectra over this region. An example of such a spectrum is given in Fig. 8. It exhibits the ammonium sulfate absorption band around  $1115\text{ cm}^{-1}$ ; but also a clear slope from  $750$  to  $1000\text{ cm}^{-1}$ . This slope appears together with the ammonium sulfate absorption band in refractive indices of water soluble aerosol, reported in Volz (1972a,b) and Shettle and Fenn (1979). The time and location of the ammonium sulfate plume coincides very well with increased AOD in MODIS, LIDAR and AERONET measurements (Kim et al., 2007). The peak in June/July is explained by the availability of ammonia and favorable stable meteorological conditions in terms of build up and growth of aerosols (Kim et al., 2006, 2007).

## Aerosol type specification in the infrared

L. Clarisse et al.

Title Page

Abstract

Introduction

Conclusions

References

Tables

Figures

◀

▶

◀

▶

Back

Close

Full Screen / Esc

Printer-friendly Version

Interactive Discussion



Globally, ammonium sulfate was not confidently detected anywhere else over background noise and interferences of dust and smoke.

## 4.6 Smoke

Smoke from biomass burning consists of 50–70 % of organic and black carbon, representing less than 5 % of burned carbon. In addition secondary particles are also formed within smoke plumes. The majority of smoke particles is in the accumulation mode ( $< 1 \mu\text{m}$  diameter) and efficiently absorb and scatter solar radiation. A non-negligible fraction ( $\sim 10\%$  in mass) of coarse mode particles consisting of ash, soil, carbons and partially combusted biomass with sizes is in the coarse mode (Reid et al., 2005a,b).

This suggests the possibility of interaction with infrared radiation. One of the few laboratory measurements of smoke particles in the infrared (Sutherland and Khanna, 1991) reports significant extinction between  $1000$  and  $1800 \text{ cm}^{-1}$ , see Fig. 10. Also IASI observations of smoke particles have been reported (Clarisse et al., 2010a). Since the launch of IASI, the most clear observations of smoke particles were probably made in plumes from the Australian bush fires of 2009, where a global drop in the baseline of  $\sim 10 \text{ K}$  (and  $\sim 20 \text{ K}$  between  $1050$  and  $1250 \text{ cm}^{-1}$ ) was observed (Clarisse et al., 2011). Although in this case, arguably, part of the observed signature was also due to the sum of all enhanced trace gas absorptions (e.g. from large molecules as PAN and acetic acid). Other observations of smoke with IASI were reported in Köhler et al. (2011), who point out the importance of thermal contrast and the fact that downwelling infrared radiance is much more affected by the presence of smoke than upwelling radiance.

For the covariance matrices we have used the same ones as for the detection of ammonium sulfate, with again land/ocean separation and cloud filtering. A Jacobian was generated from a simulation using the refractive indices of smoke from a mixed weed sample reported in Sutherland and Khanna (1991). While the detection is noisy on an individual spectrum basis, it picks up (aged) smoke plumes over the South Atlantic and Indian ocean especially in September and October as shown in Fig. 11 for October 2010. It is well known that fires in Southern Africa and South America peak in

### Aerosol type specification in the infrared

L. Clarisse et al.

Title Page

Abstract

Introduction

Conclusions

References

Tables

Figures

◀

▶

◀

▶

Back

Close

Full Screen / Esc

Printer-friendly Version

Interactive Discussion



these months. Also the transport pattern from West to East matches well with earlier observations (Edwards et al., 2006; Giglio et al., 2006; Roy et al., 2008).

## 5 Conclusions

In this paper we have presented a unified aerosol detection scheme based on a primary relative and secondary absolute distance criterion. The primary criterion uses classical linear discrimination analysis, and generalizes previously reported detection scheme using optimal estimation and PCA's. The secondary criterion was used here to filter out false detections which becomes necessary when the underlying probability distributions depart from normality. We have demonstrated the methods on IASI observations using six different types of aerosol namely volcanic ash, windblown sand, ice crystals, sulfuric acid droplets, ammonium sulfate and smoke particles. For each of these we have introduced small adaptations in the exact implementation, mainly in the way the Jacobian and covariance matrices were generated. It is clear that there are lot of different variations, which will work equally well. The presented results should therefore be seen as proof of concept rather than finished products.

It would indeed be a natural step to use the presented first generation products as a basis for a second generation product. As we demonstrated for sand detection, first generation products can be used to build better covariance matrices. Other improvements could include making use of larger spectral range (in particular the window between  $2000\text{--}2200\text{ cm}^{-1}$ ) and to make more use of space and time differentiated covariance matrices. Improvements outside the current detection framework include making use of some of the more advanced techniques of class discrimination. Indeed, we have only implemented here what is essentially the most basic form of class discrimination, while the state of the art is vast and highly advanced (McLachlan, 2004). Also note that nothing in the method is IASI specific, so that our techniques can easily be applied to measurements of other high spectral resolution infrared sounders (TES, AIRS, GOSAT, ...).

### Aerosol type specification in the infrared

L. Clarisse et al.

Title Page

Abstract

Introduction

Conclusions

References

Tables

Figures

◀

▶

◀

▶

Back

Close

Full Screen / Esc

Printer-friendly Version

Interactive Discussion



## Aerosol type specification in the infrared

L. Clarisse et al.

Title Page

Abstract

Introduction

Conclusions

References

Tables

Figures

◀

▶

◀

▶

Back

Close

Full Screen / Esc

Printer-friendly Version

Interactive Discussion



The results exceed expectations, especially with respect to the global longterm detection of  $\text{H}_2\text{SO}_4$  both from large and sustained eruptions. Most effort has been spent on the detections of ash and sand and these would not require too much work to implement in an operational setting. The demonstration of smoke and ammonia sulfate detection was unforeseen, especially since these aerosol consist mainly of small particles ( $< 1 \mu\text{m}$ ) and are located in the lower troposphere. Also note that it is possible for multiple aerosol types to be detected in the same observation, provided that their respective spectral signatures cover at least partially different spectral regions.

Notably absent in the current scheme are regular (water) clouds and sea spray. While we have not attempted the detection of regular clouds, clouds do not have a pronounced spectral signature in the infrared, and we therefore do not expect the current scheme to be easily adaptable for their detection. Sea spray on the other hand does have a marked, but slowly varying spectral signature (Irshad et al., 2009). We have attempted detection of sea spray but no convincing results emerged, likely due to a combination of (1) the use of too small spectral range and (2) constructed covariance matrices as sea spray is omnipresent, (3) low thermal contrast over oceans and (4) no obvious test cases of enhanced loadings.

Boundary layer aerosols and fine mode particles are preferentially detected in the shortwave, and this is one of the reasons that the majority of aerosol remote sensing makes use of shortwave radiation. However, the thermal infrared offers some marked advantages, especially for the sounding of coarse mode aerosols. Examples include its potential to measure size, altitude and as we have demonstrated here, type specification. The results presented here demonstrate the enormous potential of infrared aerosol sensing, but at the same time leads us to conclude that it is largely unexplored.

*Acknowledgements.* IASI has been developed and built under the responsibility of the Centre National d'Etudes Spatiales (CNES, France). It is flown onboard the Metop satellites as part of the EUMETSAT Polar System. The IASI L1 data are received through the EUMETCast near real time data distribution service. L. Clarisse and P.-F. Coheur are respectively Postdoctoral Researcher (Chargé de Recherches) and Research Associate (Chercheur Qualifié) with F.R.S.-FNRS. C. Clerbaux is grateful to CNES for scientific collaboration and financial support. The

research in Belgium was funded by the F.R.S.-FNRS (M.I.S. nF.4511.08), the Belgian State Federal Office for Scientific, Technical and Cultural Affairs and the European Space Agency (ESA-Prodex arrangements and the Support to Aviation Control Service (SACS+) project). We also acknowledge financial support from the “Actions de Recherche Concertées” (Communauté Française de Belgique).

## References

- Ackerman, S. A.: Using the radiative temperature difference at 3.7 and 11  $\mu\text{m}$  to tract dust outbreaks, *Remote. Sens. Environ.*, 27, 129–133, doi:10.1016/0034-4257(89)90012-6, 1989. 26874
- Ackerman, S. A.: Remote sensing aerosols using satellite infrared observations, *J. Geophys. Res.*, 102, 17069–17079, doi:10.1029/96JD03066, 1997. 26874
- Ackerman, S. A. and Strabala, K. I.: Satellite remote sensing of  $\text{H}_2\text{SO}_4$  aerosol using the 8- to 12- $\mu\text{m}$  window region: application to Mount Pinatubo, *J. Geophys. Res.*, 99, 18639–18649, doi:10.1029/94JD01331, 1994. 26889
- Ackerman, S. A., Strabala, K. I., Menzel, W. P., Frey, R. A., Moeller, C. C., and Gumley, L. E.: Discriminating clear sky from clouds with MODIS, *J. Geophys. Res.*, 103, 32141–32157, doi:10.1029/1998JD200032, 1998. 26874
- Adams, P. J., Seinfeld, J. H., and Koch, D. M.: Global concentrations of tropospheric sulfate, nitrate, and ammonium aerosol simulated in a general circulation model, *J. Geophys. Res.*, 104, 13791–13823, doi:10.1029/1999JD900083, 1999. 26898
- Antonelli, P., Revercomb, H. E., Sromovsky, L. A., Smith, W. L., Knuteson, R. O., Tobin, D. C., Garcia, R. K., Howell, H. B., Huang, H.-L., and Best, F. A.: A principal component noise filter for high spectral resolution infrared measurements, *J. Geophys. Res.*, 109, D23102, doi:10.1029/2004JD004862, 2004. 26879
- Atkinson, N. C., Hilton, F. I., Illingworth, S. M., Eyre, J. R., and Hultberg, T.: Potential for the use of reconstructed IASI radiances in the detection of atmospheric trace gases, *Atmos. Meas. Tech.*, 3, 991–1003, doi:10.5194/amt-3-991-2010, 2010. 26879
- August, T., Klaes, D., Schlüssel, P., Hultberg, T., Crapeau, M., Arriaga, A., O’Carroll, A., Copens, D., Munro, R., and Calbet, X.: IASI on Metop-A: operational level 2 retrievals after five

## Aerosol type specification in the infrared

L. Clarisse et al.

Title Page

Abstract

Introduction

Conclusions

References

Tables

Figures

◀

▶

◀

▶

Back

Close

Full Screen / Esc

Printer-friendly Version

Interactive Discussion



## Aerosol type specification in the infrared

L. Clarisse et al.

Title Page

Abstract

Introduction

Conclusions

References

Tables

Figures

◀

▶

◀

▶

Back

Close

Full Screen / Esc

Printer-friendly Version

Interactive Discussion



years in orbit, *J. Quant. Spectrosc. Ra.*, 113, 1340–1371, doi:10.1016/j.jqsrt.2012.02.028, 2012. 26888

Bauman, J., Russell, P. B., Geller, M. A., and Hamill, P.: A stratospheric aerosol climatology from SAGE II and CLAES measurements: 2. Results and comparisons, 1984–1999, *J. Geophys. Res.*, 108, 4383, doi:10.1029/2002JD002993, 2003. 26889

Beer, R. and Norton, R.: Analysis of spectra using correlation functions, *Appl. Optics*, 27, 1255–1261, doi:10.1364/AO.27.001255, 1987. 26879

Bluth, G. J. S. and Carn, S. A.: Exceptional sulfur degassing from Nyamuragira volcano, 1979–2005, *Int. J. Remote Sens.*, 29, 6667–6685, doi:10.1080/01431160802168434, 2008. 26892

Boer, G. J., Sokolik, I. N., and Martin, S. T.: Infrared optical constants of aqueous sulfate–nitrate–ammonium multi-component tropospheric aerosols from attenuated total reflectance measurements – Part I: Results and analysis of spectral absorbing features, *J. Quant. Spectrosc. Ra.*, 108, 17–38, doi:10.1016/j.jqsrt.2007.02.017, 2007. 26890, 26898

Bourassa, A., Degenstein, D. A., Elash, B. J., and Llewellyn, E. J.: Evolution of the stratospheric aerosol enhancement following the eruptions of Okmok and Kasatochi: Odin-OSIRIS measurements, *J. Geophys. Res.*, 115, D00L03, doi:10.1029/2009JD013274, 2010. 26890

Bourassa, A., Robock, A., Randel, W., Deshler, T., Rieger, L., Lloyd, N., Llewellyn, E. J., and Degenstein, D.: Large volcanic aerosol load in the stratosphere linked to Asian monsoon transport, *Science*, 337, 78–81, doi:10.1126/science.1219371, 2012. 26891

Carboni, E., Thomas, G. E., Sayer, A. M., Siddans, R., Poulsen, C. A., Grainger, R. G., Ahn, C., Antoine, D., Bevan, S., Braak, R., Brindley, H., DeSouza-Machado, S., Deuzé, J. L., Diner, D., Ducos, F., Grey, W., Hsu, C., Kalashnikova, O. V., Kahn, R., North, P. R. J., Salustro, C., Smith, A., Tanré, D., Torres, O., and Veihelmann, B.: Intercomparison of desert dust optical depth from satellite measurements, *Atmos. Meas. Tech.*, 5, 1973–2002, doi:10.5194/amt-5-1973-2012, 2012. 26893

Carn, S. and Bluth, G.: Prodigious sulfur dioxide emissions from Nyamuragira volcano, D.R. Congo, *Geophys. Res. Lett.*, 30, 2211, doi:10.1029/2003GL018465, 2003. 26892

Carn, S., Strow, L., de Souza-Machado, S., Edmonds, Y., and Hannon, S.: Quantifying tropospheric volcanic emissions with AIRS: the 2002 eruption of Mt. Etna (Italy), *Geophys. Res. Lett.*, 32, L02301, doi:10.1029/2004GL021034, 2005. 26874

Carn, S. A., Krueger, A. J., Krotkov, N. A., Yang, K., and Evans, K.: Tracking volcanic sulfur dioxide clouds for aviation hazard mitigation, *Nat. Hazards*, 51, 325–343, doi:10.1007/s11069-008-9228-4, 2009. 26889

**Aerosol type  
specification in the  
infrared**

L. Clarisse et al.

Title Page

Abstract

Introduction

Conclusions

References

Tables

Figures

◀

▶

◀

▶

Back

Close

Full Screen / Esc

Printer-friendly Version

Interactive Discussion



- Casadevall, T. J. (Ed.): Proceedings of the First International Symposium on Volcanic Ash and Aviation Safety, Seattle, Washington, July 1991, 1994. 26895
- Clarisse, L., Coheur, P. F., Prata, A. J., Hurtmans, D., Razavi, A., Phulpin, T., Hadji-Lazaro, J., and Clerbaux, C.: Tracking and quantifying volcanic SO<sub>2</sub> with IASI, the September 2007 eruption at Jebel at Tair, Atmos. Chem. Phys., 8, 7723–7734, doi:10.5194/acp-8-7723-2008, 2008. 26874, 26878
- Clarisse, L., Clerbaux, C., Dentener, F., Hurtmans, D., and Coheur, P.-F.: Global ammonia distribution derived from infrared satellite observations, Nat. Geosci., 2, 479–483, doi:10.1038/ngeo551, 2009. 26874
- Clarisse, L., Hurtmans, D., Prata, A. J., Karagulian, F., Clerbaux, C., Mazière, M. D., and Coheur, P.-F.: Retrieving radius, concentration, optical depth, and mass of different types of aerosols from high-resolution infrared nadir spectra, Appl. Optics, 49, 3713–3722, doi:10.1364/AO.49.003713, 2010a. 26877, 26887, 26888, 26890, 26899
- Clarisse, L., Prata, F., Lacour, J.-L., Hurtmans, D., Clerbaux, C., and Coheur, P.-F.: A correlation method for volcanic ash detection using hyperspectral infrared measurements, Geophys. Res. Lett., 37, L19806, doi:10.1029/2010GL044828, 2010b. 26879, 26881, 26885, 26886, 26896, 26897
- Clarisse, L., R'Honi, Y., Coheur, P.-F., Hurtmans, D., and Clerbaux, C.: Thermal infrared nadir observations of 24 atmospheric gases, Geophys. Res. Lett., 38, L10802, doi:10.1029/2011GL047271, 2011. 26876, 26899
- Clarisse, L., Hurtmans, D., Clerbaux, C., Hadji-Lazaro, J., Ngadi, Y., and Coheur, P.-F.: Retrieval of sulphur dioxide from the infrared atmospheric sounding interferometer (IASI), Atmos. Meas. Tech., 5, 581–594, doi:10.5194/amt-5-581-2012, 2012. 26890, 26891, 26892
- Clark, R. N.: Chapter 1: Spectroscopy of rocks and minerals, and principles of spectroscopy, in: Manual of Remote Sensing, Volume 3, Remote Sensing for the Earth Sciences, edited by: Rencz, A., John Wiley and Sons, New York, 3–58, available at: <http://speclab.cr.usgs.gov/PAPERS.refl-mrs/> (last access: October 2012), 1999. 26893
- Clerbaux, C., Boynard, A., Clarisse, L., George, M., Hadji-Lazaro, J., Herbin, H., Hurtmans, D., Pommier, M., Razavi, A., Turquety, S., Wespes, C., and Coheur, P.-F.: Monitoring of atmospheric composition using the thermal infrared IASI/MetOp sounder, Atmos. Chem. Phys., 9, 6041–6054, doi:10.5194/acp-9-6041-2009, 2009. 26873

**Aerosol type  
specification in the  
infrared**

L. Clarisse et al.

Title Page

Abstract

Introduction

Conclusions

References

Tables

Figures

◀

▶

◀

▶

Back

Close

Full Screen / Esc

Printer-friendly Version

Interactive Discussion



Coheur, P.-F., Clarisse, L., Turquety, S., Hurtmans, D., and Clerbaux, C.: IASI measurements of reactive trace species in biomass burning plumes, *Atmos. Chem. Phys.*, 9, 5655–5667, doi:10.5194/acp-9-5655-2009, 2009. 26876

Corradini, S., Merucci, L., Prata, A. J., and Piscini, A.: Volcanic ash and SO<sub>2</sub> in the 2008 Kasatochi eruption: retrievals comparison from different IR satellite sensors, *J. Geophys. Res.*, 115, D00L21, doi:10.1029/2009JD013634, 2010. 26878

DeSouza-Machado, S., Strow, L., Hannon, S., and Motteler, H.: Infrared dust spectral signatures from AIRS, *Geophys. Res. Lett.*, 33, L03801, doi:10.1029/2005GL024364, 2006. 26874

DeSouza-Machado, S. G., Strow, L. L., Imbiriba, B., K. McCann, K., Hoff, R. M., Hannon, S. E., Martins, J. V., Tanré, D., Deuzé, J. L., Ducos, F., and Torres, O.: Infrared retrievals of dust using AIRS: comparisons of optical depths and heights derived for a North African dust storm to other collocated EOS A-Train and surface observations, *J. Geophys. Res.*, 115, D15201, doi:10.1029/2009JD012842, 2010. 26878, 26893

Doeringer, D.: Observation of sulphate aerosols and SO<sub>2</sub> from volcanic eruptions using data from the Atmospheric Chemistry Experiment (ACE), Master's thesis, University of York, UK, 2011. 26891

Doeringer, D., Eldering, A., Boone, C. D., Abad, G. G., and Bernath, P. F.: Observation of sulfate aerosols and SO<sub>2</sub> from the Sarychev volcanic eruption using data from the Atmospheric Chemistry Experiment (ACE), *J. Geophys. Res.*, 117, D03203, doi:10.1029/2011JD016556, 2012. 26890, 26891

Downing, H. D., Pinkley, L. W., Sethna, P. P., and Williams, D.: Optical constants of ammonium sulfate in the infrared, *J. Opt. Soc. Am.*, 67, 186–190, doi:10.1364/JOSA.67.000186, 1977. 26898

Earle, M. E., Pancescu, R. G., Cosic, B., Zsetsky, A. Y., and Sloan, J. J.: Temperature-dependent complex indices of refraction for crystalline (NH<sub>4</sub>)<sub>2</sub>SO<sub>4</sub>, *J. Phys. Chem. A*, 110, 13022–13028, doi:10.1021/jp064704s, 2006. 26898, 26925

Echle, G., von Clarmann, T., and Oelhaf, H.: Optical and microphysical parameters of the Mt. Pinatubo aerosol as determined from MIPAS-B mid-IR limb emission spectra, *J. Geophys. Res.*, 103, 19193–19211, doi:10.1029/98JD01363, 1998. 26889, 26890

Edwards, D. P., Emmons, L. K., Gille, J. C., Chu, A., Attié, J.-L., Giglio, L., Wood, S. W., Haywood, J., Deeter, M. N., Massie, S. T., Ziskin, D. C., and Drummond, J. R.: Satellite-observed pollution from Southern Hemisphere biomass burning, *J. Geophys. Res.*, 111, D14312, doi:10.1029/2005JD006655, 2006. 26900

## Aerosol type specification in the infrared

L. Clarisse et al.

Title Page

Abstract

Introduction

Conclusions

References

Tables

Figures

◀

▶

◀

▶

Back

Close

Full Screen / Esc

Printer-friendly Version

Interactive Discussion



Ellrod, G., Connell, B., and Hillger, D.: Improved detection of airborne volcanic ash using multispectral infrared satellite data, *J. Geophys. Res.*, 108, 4356, doi:10.1029/2002JD002802, 2003. 26874

Flaud, J.-M., Lafferty, W., and Sams, R.: Line intensities for the  $\nu_1$ ,  $\nu_3$ , and  $\nu_1 + \nu_3$  bands of  $^{34}\text{SO}_2$ , *J. Quant. Spectrosc. Ra.*, 110, 669–674, doi:10.1016/j.jqsrt.2008.12.003, 2009. 26890

Forster, P., Ramaswamy, V., Artaxo, P., Bernsten, T., Betts, R., Fahey, D., Haywood, J., Lean, J., Lowe, D., Myhre, G., Nganga, J., Prinn, R., Raga, G., Schulz, M., and Dorland, R. V.: Changes in atmospheric constituents and in radiative forcing, in: *Climate Change 2007: The Physical Science Basis, Contribution of Working Group I to the Fourth Assessment Report of the Intergovernmental Panel on Climate Change*, edited by: Solomon, S., Qin, D., Manning, M., Chen, Z., Marquis, M., Averyt, K., Tignor, M., and Miller, H., Cambridge University Press, UK and New York, NY, USA, 129–234, available at: [http://www.ipcc.ch/publications\\_and\\_data/ar4/wg1/en/contents.html](http://www.ipcc.ch/publications_and_data/ar4/wg1/en/contents.html) (last access: October 2012), 2007. 26872

Gangale, G., Prata, A., and Clarisse, L.: The infrared spectral signature of volcanic ash determined from high-spectral resolution satellite measurements, *Remote. Sens. Environ.*, 114, 414–425, doi:10.1016/j.rse.2009.09.007, 2010. 26875, 26878, 26896

Gassó, S., Grassian, V., and Miller, R.: Interactions between mineral dust, climate, and ocean ecosystems, *Elements*, 6, 247–252, doi:10.2113/gselements.6.4.247, 2010. 26892

Giglio, L., Csiszar, I., and Justice, C. O.: Global distribution and seasonality of active fires as observed with the terra and aqua Moderate Resolution Imaging Spectroradiometer (MODIS) sensors, *J. Geophys. Res.*, 111, G02016, doi:10.1029/2005JG000142, 2006. 26900

Grainer, R., Lambert, A., Taylor, F., Remedios, J., Rodgers, C., and Corney, M.: Infrared absorption by volcanic stratospheric aerosols observed by ISAMS, *Geophys. Res. Lett.*, 20, 1283–1286, doi:10.1029/93GL00823, 1993. 26889, 26890

Haladay, T. and Stephens, G.: Characteristics of tropical thin cirrus clouds deduced from joint CloudSat and CALIPSO observations, *J. Geophys. Res.*, 114, D00A25, doi:10.1029/2008JD010675, 2009. 26888

Hamill, P., Turco, R., Kiang, C., Toon, O., and Whitten, R.: An analysis of various nucleation mechanisms for sulfate particles in the stratosphere, *J. Aerosol Sci.*, 13, 561–585, doi:10.1016/0021-8502(82)90021-0, 1982. 26889

- Hansen, J., Sato, M., Kharecha, P., and von Schuckmann, K.: Earth's energy imbalance and implications, *Atmos. Chem. Phys.*, 11, 13421–13449, doi:10.5194/acp-11-13421-2011, 2011. 26872
- 5 Haywood, J. and Boucher, O.: Estimates of the direct and indirect radiative forcing due to tropospheric aerosols: a review, *Rev. Geophys.*, 38, 513–543, doi:10.1029/1999RG000078, 2000. 26873
- 10 Haywood, J. M., Jones, A., Clarisse, L., Bourassa, A., Barnes, J., Telford, P., Bellouin, N., Boucher, O., Agnew, P., Clerbaux, C., Coheur, P., Degenstein, D., and Braesicke, P.: Observations of the eruption of the Sarychev volcano and simulations using the HadGEM2 climate model, *J. Geophys. Res.*, 115, D21212, doi:10.1029/2010JD014447, 2010. 26890, 26891
- Hess, M., Koepke, P., and Schult, I.: Optical properties of aerosols and clouds: The software package OPAC, *B. Am. Meteorol. Soc.*, 79, 831–844, doi:10.1175/1520-0477(1998)079<0831:OPOAAC>2.0.CO;2, 1998. 26925
- 15 Hilton, F., Armante, R., August, T., Barnet, C., Bouchard, A., Camy-Peyret, C., Capelle, V., Clarisse, L., Clerbaux, C., Coheur, P.-F., Collard, A., Crevoisier, C., Dufour, G., Edwards, D., Fajjan, F., Fourrié, N., Gambacorta, A., Goldberg, M., Guidard, V., Hurtmans, D., Illingworth, S., Jacquinet-Husson, N., Kerzenmacher, T., Klaes, D., Lavanant, L., Masiello, G., Matricardi, M., McNally, A., Newman, S., Pavelin, E., Payan, S., Péquignot, E., Peyridieu, S., Phulpin, T., Remedios, J., Schlüssel, P., Serio, C., Strow, L., Stubenrauch, C., Taylor, J., Tobin, D., Wolf, W., and Zhou, D.: Hyperspectral Earth observation from IASI: five years of accomplishments, *B. Am. Meteorol. Soc.*, 93, 347–370, doi:10.1175/BAMS-D-11-00027.1, 2011. 26873
- 20 Huang, H.-L. and Antonelli, P.: Application of principal component analysis to high-resolution infrared measurement compression and retrieval, *J. Appl. Meteorol.*, 40, 365–388, doi:10.1175/1520-0450(2001)040<0365:AOPCAT>2.0.CO;2, 2001. 26879
- 25 Hunt, G.: Spectroscopic properties of rocks and minerals, in: *Handbook of Physical Properties of Rocks*, edited by: Carmichael, R., CRC, Boca Raton, Florida, 295–385, 1982. 26893
- Hurley, J., Dudhia, A., and Grainger, R. G.: Cloud detection for MIPAS using singular vector decomposition, *Atmos. Meas. Tech.*, 2, 533–547, doi:10.5194/amt-2-533-2009, 2009. 26879
- 30 Hurtmans, D., Coheur, P.-F., Wespes, C., Clarisse, L., Scharf, O., Clerbaux, C., Hadji-Lazaro, J., George, M., and Turquety, S.: FORLI radiative transfer and retrieval code for IASI, *J. Quant. Spectrosc. Ra.*, 113, 1391–1408, doi:10.1016/j.jqsrt.2012.02.036, 2012. 26876

---

**Aerosol type  
specification in the  
infrared**L. Clarisse et al.

---

[Title Page](#)[Abstract](#)[Introduction](#)[Conclusions](#)[References](#)[Tables](#)[Figures](#)[◀](#)[▶](#)[◀](#)[▶](#)[Back](#)[Close](#)[Full Screen / Esc](#)[Printer-friendly Version](#)[Interactive Discussion](#)

---

**Aerosol type  
specification in the  
infrared**L. Clarisse et al.

---

[Title Page](#)[Abstract](#)[Introduction](#)[Conclusions](#)[References](#)[Tables](#)[Figures](#)[◀](#)[▶](#)[◀](#)[▶](#)[Back](#)[Close](#)[Full Screen / Esc](#)[Printer-friendly Version](#)[Interactive Discussion](#)

Inoue, T.: On the temperature and effective emissivity determination of semi-transparent cirrus clouds by bi-spectral measurements in the 10  $\mu\text{m}$  window region, *J. Meteorol. Soc. Jpn.*, 63, 88–98, 1985. 26874, 26887

Irshad, R., Grainger, R. G., Peters, D. M., McPheat, R. A., Smith, K. M., and Thomas, G.: Laboratory measurements of the optical properties of sea salt aerosol, *Atmos. Chem. Phys.*, 9, 221–230, doi:10.5194/acp-9-221-2009, 2009. 26901

Jolliffe, I.: *Principal Component Analysis*, Springer, New York, 2002. 26879

Kahn, B., Eldering, A., Clough, S., Fetzer, E., Fishbein, E., Gunson, M., Lee, S.-Y., Lester, P., and Realmuto, V.: Near micron-sized cirrus cloud particles in high-resolution infrared spectra: an orographic case study, *Geophys. Res. Lett.*, 30, 1441, doi:10.1029/2003GL016909, 2003. 26874, 26888

Karagulian, F., Clarisse, L., Clerbaux, C., Prata, A. J., Hurtmans, D., and Coheur, P. F.: Detection of volcanic  $\text{SO}_2$ , ash and  $\text{H}_2\text{SO}_4$  using the IASI sounder, *J. Geophys. Res.*, 115, D00L02, doi:10.1029/2009JD012786, 2010. 26890

Kaufman, Y., Tanré, D., and Boucher, O.: A satellite view of aerosols in the climate system, *Nature*, 419, 215–223, doi:10.1038/nature01091, 2002. 26873

Kim, J., Yoon, S.-C., Jefferson, A., and Kim, S.-W.: Aerosol hygroscopic properties during Asian dust, pollution, and biomass burning episodes at Gosan, Korea in April 2001, *Atmos. Environ.*, 40, 1550–1560, doi:10.1016/j.atmosenv.2005.10.044, 2006. 26898

Kim, S.-W., Yoon, S.-C., Kim, J., and Kim, S.-Y.: Seasonal and monthly variations of columnar aerosol optical properties over east Asia determined from multi-year MODIS, LIDAR, and AERONET Sun/sky radiometer measurements, *Atmos. Environ.*, 41, 1634–1651, doi:10.1016/j.atmosenv.2006.10.044, 2007. 26898

Klüser, L., Martynenko, D., and Holzer-Popp, T.: Thermal infrared remote sensing of mineral dust over land and ocean: a spectral SVD based retrieval approach for IASI, *Atmos. Meas. Tech.*, 4, 757–773, doi:10.5194/amt-4-757-2011, 2011. 26879

Klüser, L., Erbertseder, T., and Meyer-Arne, J.: Observation of volcanic ash from Puyehue-Cordón Caulle with IASI, *Atmos. Meas. Tech. Discuss.*, 5, 4249–4283, doi:10.5194/amtd-5-4249-2012, 2012. 26896, 26897

Köhler, C., Trautmann, T., Lindermeier, E., Vreeling, W., Lieke, K., Kandler, K., Weinzierl, B., Groß, S., Tesche, M., and Wendisch, M.: Thermal IR radiative properties of mixed mineral dust and biomass aerosol during SAMUM-2, *Tellus B*, 63, 751–769, doi:10.1111/j.1600-0889.2011.00563.x, 2011. 26899

## Aerosol type specification in the infrared

L. Clarisse et al.

Title Page

Abstract

Introduction

Conclusions

References

Tables

Figures

◀

▶

◀

▶

Back

Close

Full Screen / Esc

Printer-friendly Version

Interactive Discussion



- Kondratyev, K., Ivlev, L., Krapivin, V. F., and Varotsos, C. (Eds.): Atmospheric Aerosol Properties: Formation, Processes and Impacts, Springer, Berlin, 2005. 26872
- Kravitz, B., Robock, A., Bourassa, A., Deshler, T., Wu, D., Mattis, I., Finger, F., Hoffmann, A., Ritter, C., Bitar, L., Duck, T. J., and Barnes, J. E.: Simulation and observations of stratospheric aerosols from the 2009 Sarychev volcanic eruption, *J. Geophys. Res.*, 116, D18211, doi:10.1029/2010JD015501, 2011. 26890
- Krotkov, N., Schoeberl, M., Morris, G., Carn, S., and Yang, K.: Dispersion and lifetime of the SO<sub>2</sub> cloud from the August 2008 Kasatochi eruption, *J. Geophys. Res.*, 115, D00L20, doi:10.1029/2010JD013984, 2010. 26891
- Lamberta, A., Grainger, R. G., Rodgers, C. D., Taylor, F. W., Mergenthaler, J. L., Kumer, J. B., and Massie, S. T.: Global evolution of the Mt. Pinatubo volcanic aerosols observed by the infrared limb-sounding instruments CLAES and ISAMS on the upper atmosphere research satellite, *J. Geophys. Res.*, 102, 1495–1512, doi:10.1029/96JD00096, 1997. 26889
- Legrand, M., Plana-Fattori, A., and N'doumé, C.: Satellite detection of dust using the IR imagery of Meteosat 1. Infrared difference dust index, *J. Geophys. Res.*, 106, 18251–18274, doi:10.1029/2000JD900749, 2001. 26881
- Li, J., Huang, H., Liu, C., Yang, P., Schmit, T., Wei, H., Weisz, E., Guan, L., and Menzel, W.: Retrieval of cloud microphysical properties from MODIS and AIRS, *J. Appl. Meteorol.*, 44, 1526–1543, doi:10.1175/JAM2281.1, 2005. 26878, 26888
- Li, Z., Zhao, X., Kahn, R., Mishchenko, M., Remer, L., Lee, K.-H., Wang, M., Laszlo, I., Nakajima, T., and Maring, H.: Uncertainties in satellite remote sensing of aerosols and impact on monitoring its long-term trend: a review and perspective, *Ann. Geophys.*, 27, 2755–2770, doi:10.5194/angeo-27-2755-2009, 2009. 26873
- Li, Z., Niu, F., Fan, J., Liu, Y., Rosenfeld, D., and Ding, Y.: Long-term impacts of aerosols on the vertical development of clouds and precipitation, *Nat. Geosci.*, 4, 888–894, doi:10.1038/ngeo1313, 2011. 26873
- Long, C. S. and Stowe, L. L.: Using the NOAA/AVHRR to study stratospheric aerosol optical thicknesses following the Mt. Pinatubo Eruption, *Geophys. Res. Lett.*, 21, 2215–2218, doi:10.1029/94GL01322, 1994. 26889
- Lynch, D., Sassen, K., Starr, D., and Stephens, G. (Eds.): *Cirrus*, Oxford University Press, New York, 2002. 26887
- Mace, G. G., Zhang, Y., Platnick, S., King, M. D., Minnis, P., and Yang, P.: Evaluation of cirrus cloud properties derived from MODIS data using cloud properties derived from

## Aerosol type specification in the infrared

L. Clarisse et al.

Title Page

Abstract

Introduction

Conclusions

References

Tables

Figures

◀

▶

◀

▶

Back

Close

Full Screen / Esc

Printer-friendly Version

Interactive Discussion



ground-based observations collected at the ARM SGP site, *J. Appl. Meteor.*, 44, 221–240, doi:10.1175/JAM2193.1, 2005. 26888

Martin, S. T., Hung, H.-M., Park, R. J., Jacob, D. J., Spurr, R. J. D., Chance, K. V., and Chin, M.: Effects of the physical state of tropospheric ammonium-sulfate-nitrate particles on global aerosol direct radiative forcing, *Atmos. Chem. Phys.*, 4, 183–214, doi:10.5194/acp-4-183-2004, 2004. 26898

Masiello, G., Matricardi, M., Rizzi, R., and Serio, C.: Homomorphism between cloudy and clear spectral radiance in the 800–900-cm<sup>-1</sup> atmospheric window region, *Appl. Optics*, 41, 965–973, doi:10.1364/AO.41.000965, 2002. 26879

Mazzocchi, M., Hansstein, F., and Ragona, M.: The 2010 volcanic ash cloud and its financial impact on the European airline industry, *CESifo Forum*, 11, 92–100, 2010. 26895

McLachlan, G. J.: *Discriminant Analysis and Statistical Pattern Recognition*, Wiley, Hoboken, New Jersey, 2004. 26882, 26900

Miller, T. and Casadevall, T.: Volcanic ash hazards to aviation, in: *Encyclopedia of Volcanoes*, edited by: Sigurdsson, H., Academic Press, San Diego, 915–930, 2000. 26895

Newman, S. M., Clarisse, L., Hurtmans, D., Marenco, F., Johnson, B., Turnbull, K., Have-  
mann, S., Baran, A. J., O'Sullivan, D., and Haywood, J.: A case study of observations of  
volcanic ash from the Eyjafjallajökull eruption: 2. airborne and satellite radiative measure-  
ments, *J. Geophys. Res.*, 117, D00U13, doi:10.1029/2011JD016780, 2012. 26875, 26896

NOAA-NASA-USAF: *US Standard Atmosphere 1976*, US Government Printing Office, Wash-  
ington, DC, 1976. 26887

OFCEM (Ed.): *Proceedings of the second international conference on volcanic ash and aviation  
safety*, Alexandria, Virginia, June 2004, US Department of Commerce/National Oceanic and  
Atmospheric Administration, Washington, DC, 2004. 26895

O'Neill, N. T., Perro, C., Saha, A., Lesins, G., Duck, T. J., Eloranta, E. W., Nott, G. J., Hoff-  
man, A., Karumudi, M. L., Ritter, C., Bourassa, A., Abboud, I., Carn, S. A., and Savastiouk, V.:  
Properties of Sarychev sulphate aerosols over the Arctic, *J. Geophys. Res.*, 117, D04203,  
doi:10.1029/2011JD016838, 2012. 26890

Parol, F., Buriez, J., Brogniez, G., and Fouquart, Y.: Information content of AVHRR channels  
4 and 5 with respect to the effective radius of cirrus cloud particles, *J. Appl. Meteorol.*, 30,  
973–984, doi:10.1175/1520-0450-30.7.973, 1991. 26874, 26887

Pavolonis, M. J. and Sieglaff, J.: *GOES-R Advanced Baseline Imager (ABI) Algorithm Theoret-  
ical Basis Document for Volcanic Ash (Detection and Height)*, Tech. rep., NOAA NESDIS

## Aerosol type specification in the infrared

L. Clarisse et al.

Title Page

Abstract

Introduction

Conclusions

References

Tables

Figures

◀

▶

◀

▶

Back

Close

Full Screen / Esc

Printer-friendly Version

Interactive Discussion

STAR, available at: [http://cimss.ssec.wisc.edu/~mpav/GOESR\\_ABI\\_ATBD\\_Aviation\\_VolAsh\\_v2.1.pdf](http://cimss.ssec.wisc.edu/~mpav/GOESR_ABI_ATBD_Aviation_VolAsh_v2.1.pdf) (last access: October 2012), 2010. 26881, 26896

Pavolonis, M. J., Feltz, W. F., Heidinger, A. K., and Gallina, G. M.: A daytime complement to the reverse absorption technique for improved automated detection of volcanic ash, *J. Atmos. Ocean. Tech.*, 23, 1422–1444, doi:10.1175/JTECH1926.1, 2006. 26874

Pergola, N., Tramutoli, V., Marchese, F., Scaffidi, I., and Lacava, T.: Improving volcanic ash cloud detection by a robust satellite technique, *Remote. Sens. Environ.*, 90, 1–22, doi:10.1016/j.rse.2003.11.014, 2004. 26881

Peyridieu, S., Chédin, A., Tanré, D., Capelle, V., Pierangelo, C., Lamquin, N., and Armante, R.: Saharan dust infrared optical depth and altitude retrieved from AIRS: a focus over North Atlantic – comparison to MODIS and CALIPSO, *Atmos. Chem. Phys.*, 10, 1953–1967, doi:10.5194/acp-10-1953-2010, 2010. 26878, 26893, 26895

Pierangelo, C., Chédin, A., Heilliette, S., Jacquinet-Husson, N., and Armante, R.: Dust altitude and infrared optical depth from AIRS, *Atmos. Chem. Phys.*, 4, 1813–1822, doi:10.5194/acp-4-1813-2004, 2004. 26893

Pierangelo, C., Mishchenko, M., Balkanski, Y., and Chedin, A.: Retrieving the effective radius of Saharan dust coarse mode from AIRS, *Geophys. Res. Lett.*, 32, L20813, doi:10.1029/2005GL023425, 2005. 26893

Pollack, J., Toon, O., and Khare, B.: Optical properties of some terrestrial rocks and glasses, *Icarus*, 19, 372–389, doi:10.1016/0019-1035(73)90115-2, 1973. 26896

Pöschl, U.: Atmospheric aerosols: composition, transformation, *Angew. Chem. Int. Edit.*, 44, 7520–7540, doi:10.1002/anie.200501122, 2005. 26872

Prasad, A. A. and Davies, R.: Detecting tropical thin cirrus using Multiangle Imaging Spectro-Radiometer's oblique cameras and modeled outgoing longwave radiation, *J. Geophys. Res.*, 117, D06208, doi:10.1029/2011JD016798, 2012. 26888

Prata, A.: Infrared radiative transfer calculations for volcanic ash clouds, *Geophys. Res. Lett.*, 16, 1293–1296, doi:10.1029/GL016i011p01293, 1989. 26874

Prata, A. J.: Satellite detection of hazardous volcanic clouds and the risk to global air traffic, *Nat. Hazards*, 51, 303–324, doi:10.1007/s11069-008-9273-z, 2009. 26896

Prata, A. and Bernardo, C.: Retrieval of volcanic SO<sub>2</sub> column abundance from Atmospheric Infrared Sounder data, *J. Geophys. Res.*, 112, D20204, doi:10.1029/2006JD007955, 2007. 26878

## Aerosol type specification in the infrared

L. Clarisse et al.

Title Page

Abstract

Introduction

Conclusions

References

Tables

Figures

◀

▶

◀

▶

Back

Close

Full Screen / Esc

Printer-friendly Version

Interactive Discussion



- Prata, A. J. and Prata, A. T.: Eyjafjallajökull volcanic ash concentrations determined using Spin Enhanced Visible and Infrared Imager measurements, *J. Geophys. Res.*, 117, D00U23, doi:10.1029/2011JD016800, 2012. 26874, 26896
- Ramanathan, V., Crutzen, P. J., Kiehl, J. T., and Rosenfeld, D.: Aerosols, climate, and the hydrological cycle, *Science*, 294, 2119–2124, doi:10.1126/science.1064034, 2007. 26873
- Reid, J. S., Eck, T. F., Christopher, S. A., Koppmann, R., Dubovik, O., Eleuterio, D. P., Holben, B. N., Reid, E. A., and Zhang, J.: A review of biomass burning emissions part III: intensive optical properties of biomass burning particles, *Atmos. Chem. Phys.*, 5, 827–849, doi:10.5194/acp-5-827-2005, 2005a. 26899
- Reid, J. S., Koppmann, R., Eck, T. F., and Eleuterio, D. P.: A review of biomass burning emissions part II: intensive physical properties of biomass burning particles, *Atmos. Chem. Phys.*, 5, 799–825, doi:10.5194/acp-5-799-2005, 2005b. 26899
- Remsberg, E.: Optical constants of concentrated aqueous ammonium sulfate, *Appl. Optics*, 12, 1389–1390, doi:10.1364/AO.12.001389, 1973. 26898
- Rencher, A.: *Methods of Multivariate Analysis (second edition)*, Wiley-Interscience, New York, 2002. 26878
- Ripley, B. D.: *Pattern recognition and neural networks*, Cambridge University Press, Cambridge (UK), 1996. 26882, 26886
- Robock, A.: Volcanic eruptions and climate, *Rev. Geophys.*, 38, 191–219, doi:10.1029/1998RG000054, 2000. 26889
- Rodgers, C.: *Inverse methods for atmospheric sounding: theory and practice, series on atmospheric, oceanic and planetary physics*, World Scientific, Singapore, 2000. 26875, 26876
- Rogers, H. L., Norton, W. A., Lambert, A., and Grainger, R. G.: Transport of Mt. Pinatubo aerosol by tropospheric synoptic-scale and stratospheric planetary-scale waves, *Q. J. Roy. Meteorol. Soc.*, 124, 193–209, doi:10.1002/qj.49712454509, 1998. 26889
- Rose, W. I. and Durant, A. J.: Fine ash content of explosive eruptions, *J. Volcanol. Geoth. Res.*, 186, 32–39, doi:10.1016/j.jvolgeores.2009.01.010, 2009. 26895
- Rose, W. I., Delene, D. J., Schneider, D. J., Bluth, G. J. S., Krueger, A. J., Sprod, I., McKee, C., Davies, H. L., and Ernst, G. G. J.: Ice in the 1994 Rabaul eruption cloud: implications for volcano hazard and atmospheric effects, *Nature*, 375, 477–479, doi:10.1038/375477a0, 1995. 26874

## Aerosol type specification in the infrared

L. Clarisse et al.

Title Page

Abstract

Introduction

Conclusions

References

Tables

Figures

◀

▶

◀

▶

Back

Close

Full Screen / Esc

Printer-friendly Version

Interactive Discussion



Rose, W. I., Bluth, G., and Watson, I.: Ice in volcanic clouds: when and where?, in: Proc. of the 2nd Int. Conf. on Volcanic Ash and Aviation Safety, OFCM, Washington, DC, Session 3, 61, 2004. 26887

Roy, D., Boschetti, L., Justice, C., and Ju, J.: The collection 5 MODIS burned area product – global evaluation by comparison with the MODIS active fire product, Remote Sens. Environ., 112, 3690–3707, doi:10.1016/j.rse.2008.05.013, 2008. 26900

Sassen, K., Wang, Z., and Liu, D.: Global distribution of cirrus clouds from CloudSat/Cloud-Aerosol Lidar and Infrared Pathfinder Satellite Observations (CALIPSO) measurements, J. Geophys. Res., 113, D00A12, doi:10.1029/2008JD009972, 2008. 26888

Schmidt, A., Ostro, B., Carslaw, K., Wilson, M., Thordarson, T., Mann, G., and Simmons, A.: Excess mortality in Europe following a future Laki-style Icelandic eruption, P. Natl. Acad. Sci. USA, 108, 15710–15715, doi:10.1073/pnas.1108569108, 2011. 26889

Segal-Rosenheimer, M., Dubowski, Y., and Linker, R.: Extraction of optical constants from mid-IR spectra of small aerosol particles, J. Quant. Spectrosc. Ra., 110, 415–426, doi:10.1016/j.jqsrt.2009.01.005, 2009. 26898

Serio, C., Lubrano, A. M., Romano, F., and Shimoda, H.: Cloud detection over sea surface by use of autocorrelation functions of upwelling infrared spectra in the 800–900-cm<sup>-1</sup> window region, Appl. Optics, 39, 3565–3572, doi:10.1364/AO.39.003565, 2000. 26879

Shettle, E. and Fenn, R.: Models for the aerosols of the lower atmosphere and the effects of humidity variations on their optical properties, Tech. rep., AFGL-TR-79-0214, United States Air Force, Air Force Systems Command, Air Force Geophysics Laboratory, Hanscom, Massachusetts, 1979. 26898, 26925

Smith, W. L., Ackerman, S. A., Revercomb, H., Huang, H., DeSlover, D. H., Feltz, W., Gumley, L., and Collard, A.: Infrared spectral absorption of nearly invisible cirrus clouds, Geophys. Res. Lett., 25, 1137–1140, doi:10.1029/97GL03491, 1998. 26888

Sokolik, I. and Toon, O.: Incorporation of mineralogical composition into models of the radiative properties of mineral aerosol from UV to IR wavelenghts, J. Geophys. Res., 104, 9423–9444, doi:10.1029/1998JD200048, 1999. 26877, 26893

Steele, H. and Hamill, P.: Effects of temperature and humidity on the growth and optical properties of sulphuric acid-water droplets in the stratosphere, J. Aerosol Sci., 12, 517–528, doi:10.1016/0021-8502(81)90054-9, 1981. 26889, 26890

**Aerosol type  
specification in the  
infrared**

L. Clarisse et al.

Title Page

Abstract

Introduction

Conclusions

References

Tables

Figures

◀

▶

◀

▶

Back

Close

Full Screen / Esc

Printer-friendly Version

Interactive Discussion



- Stenchikov, G. L., Kirchner, I., Robock, A., Graf, H.-F., Antuna, J. C., Grainger, R. G., Lambert, A., and Thomason, L.: Radiative forcing from the 1991 Mount Pinatubo volcanic eruption, *J. Geophys. Res.*, 103, 13837–13857, doi:10.1029/98JD00693, 1998. 26889
- 5 Stohl, A., Prata, A. J., Eckhardt, S., Clarisse, L., Durant, A., Henne, S., Kristiansen, N. I., Minikin, A., Schumann, U., Seibert, P., Stebel, K., Thomas, H. E., Thorsteinsson, T., Tørseth, K., and Weinzierl, B.: Determination of time- and height-resolved volcanic ash emissions and their use for quantitative ash dispersion modeling: the 2010 Eyjafjallajökull eruption, *Atmos. Chem. Phys.*, 11, 4333–4351, doi:10.5194/acp-11-4333-2011, 2011. 26895
- 10 Stowe, L. L., Carey, R. M., and Pellegrino, P. P.: Monitoring the Mt. Pinatubo aerosol layer with NOAA/11 AVHRR data, *Geophys. Res. Lett.*, 19, 159–162, doi:10.1029/91GL02958, 1992. 26889
- Strabala, K. I., Ackerman, S. A., and Menzel, W. P.: Cloud Properties inferred from 8–12 $\mu$ m Data, *J. Appl. Meteorol.*, 33, 212–229, doi:10.1175/1520-0450(1994)033<0212:CPIFD>2.0.CO;2, 1994. 26874
- 15 Stubenrauch, C. J., Chédin, A., Rädcl, G., Scott, N. A., and Serrar, S.: Cloud properties and their seasonal and diurnal variability from TOVS path-B, *J. Climate*, 19, 5531–5553, doi:10.1175/JCLI3929.1, 2006. 26888
- Sutherland, R. and Khanna, R.: Optical properties of organic-based aerosols produced by burning vegetation, *Aerosol Sci. Tech.*, 14, 331–342, doi:10.1080/02786829108959495, 1991. 26899, 26927
- 20 They, N., Campion, R., Clarisse, L., Brenot, H., van Gent, J., Dils, B., Coheur, P.-F., Roozendael, M. V., Hurtmans, D., Clerbaux, C., Tait, S., and Ferrucci, F.: Volcanic SO<sub>2</sub> fluxes derived from satellite data: a survey using OMI, GOME-2 and IASI, *Atmos. Chem. Phys. Discuss.*, submitted, 2012. 26892, 26897, 26921
- 25 Thomason, L. W., Poole, L. R., and Deshler, T.: A global climatology of stratospheric aerosol surface area density deduced from Stratospheric Aerosol and Gas Experiment II measurements: 1984–1994, *J. Geophys. Res.*, 102, 8967–8976, doi:10.1029/96JD02962, 1997. 26889
- Tisdale, R., Glandorf, D., Tolbert, M., and Toon, O.: Infrared optical constants of low-temperature H<sub>2</sub>SO<sub>4</sub> solutions representative of stratospheric sulfate aerosols, *J. Geophys. Res.*, 103, 25353–25370, doi:10.1029/98JD02457, 1998. 26890
- 30

## Aerosol type specification in the infrared

L. Clarisse et al.

Title Page

Abstract

Introduction

Conclusions

References

Tables

Figures

◀

▶

◀

▶

Back

Close

Full Screen / Esc

Printer-friendly Version

Interactive Discussion



Toon, O., Pollack, J. B., and Khare, B. N.: The optical constants of several atmospheric aerosol species: ammonium sulfate, aluminum oxide, and sodium chloride, *J. Geophys. Res.*, 81, 5733–5748, doi:10.1029/JC081i033p05733, 1976. 26898

Turco, R. P., Whitten, R. C., and Toon, O. B.: Stratospheric aerosols: observation and theory, *Rev. Geophys.*, 20, 233–279, doi:10.1029/RG020i002p00233, 1982. 26889

Vergé-Dépré, G., Legrand, M., Moulin, C., Alias, A., and François, P.: Improvement of the detection of desert dust over the Sahel using METEOSAT IR imagery, *Ann. Geophys.*, 24, 2065–2073, doi:10.5194/angeo-24-2065-2006, 2006. 26881

Vernier, J.-P., Pommereau, J.-P., Thomason, L. W., Pelon, J., Garnier, A., Deshler, T., Jumelet, J., and Nielsen, J. K.: Overshooting of clean tropospheric air in the tropical lower stratosphere as seen by the CALIPSO lidar, *Atmos. Chem. Phys.*, 11, 9683–9696, doi:10.5194/acp-11-9683-2011, 2011. 26890

Volz, F. E.: Infrared refractive index of atmospheric aerosol substances, *Appl. Optics*, 11, 755–759, doi:10.1364/AO.11.000755, 1972a. 26898, 26925

Volz, F. E.: Infrared absorption by atmospheric aerosol substances, *J. Geophys. Res.*, 77, 1017–1031, doi:10.1029/JC077i006p01017, 1972b. 26898, 26925

Volz, F. E.: Infrared optical constants of ammonium sulfate, Sahara dust; volcanic pumice and flyash, *Appl. Optics*, 12, 564–568, doi:10.1364/AO.12.000564, 1973. 26898

von Clarmann, T., Grabowski, U., and Kiefer, M.: On the role of non-random errors in inverse problems in radiative transfer and other applications, *J. Quant. Spectrosc. Ra.*, 71, 39–46, doi:10.1016/S0022-4073(01)00010-3, 2001. 26876

Walker, J. C., Dudhia, A., and Carboni, E.: An effective method for the detection of trace species demonstrated using the MetOp Infrared Atmospheric Sounding Interferometer, *Atmos. Meas. Tech.*, 4, 1567–1580, doi:10.5194/amt-4-1567-2011, 2011. 26876, 26884, 26885

Wang, T. and Dessler, A. E.: Analysis of cirrus in the tropical tropopause layer from CALIPSO and MLS data: A water perspective, *J. Geophys. Res.*, 117, D04211, doi:10.1029/2011JD016442, 2012. 26888

Wang, J., Hoffmann, A. A., Park, R. J., Jacob, D. J., and Martin, S. T.: Global distribution of solid and aqueous sulfate aerosols: effect of the hysteresis of particle phase transitions, *J. Geophys. Res.*, 113, D11206, doi:10.1029/2007JD009367, 2008. 26898

Warren, S. G. and Brandt, R. E.: Optical constants of ice from the ultraviolet to the microwave: a revised compilation, *J. Geophys. Res.*, 113, D14220, doi:10.1029/2007JD009744, 2008. 26888

## Aerosol type specification in the infrared

L. Clarisse et al.

Title Page

Abstract

Introduction

Conclusions

References

Tables

Figures

◀

▶

◀

▶

Back

Close

Full Screen / Esc

Printer-friendly Version

Interactive Discussion



- Watkin, H., Scott, T., Macadam, I., Radice, L., and Hoad, D.: Reducing the false alarm rate of a met office automatic volcanic eruption detection system, Tech. Rep. 414, UK Met Office Forecasting Research Technical Report, available at: [http://research.metoffice.gov.uk/research/nwp/publications/papers/technical\\_reports/2003/FRTR414/ABSFTR414.html](http://research.metoffice.gov.uk/research/nwp/publications/papers/technical_reports/2003/FRTR414/ABSFTR414.html) (last access: October 2012), 2003. 26881
- Wen, S. and Rose, W.: Retrieval of sizes and total masses of particles in volcanic clouds using AVHRR bands 4 and 5, *J. Geophys. Res.*, 99, 5421–5431, doi:10.1029/93JD03340, 1994. 26874
- Wu, D., Jiang, J. H., Read, W. G., Austin, R. T., Davis, C. P., Lambert, A., Stephens, G. L., Vane, D. G., and Waters, J. W.: Validation of the Aura MLS cloud ice water content measurements, *J. Geophys. Res.*, 113, D15S10, doi:10.1029/2007JD008931, 2008. 26888
- Wu, M.-L. C.: A method for remote sensing the emissivity, fractional cloud cover and cloud top temperature of high-level, thin clouds, *J. Clim. Appl. Meteorol.*, 26, 225–233, doi:10.1175/1520-0450(1987)026<0225:AMFRST>2.0.CO;2, 1987. 26874
- Wylie, D., Menzel, W., Woolf, H., and Strabala, K.: Four years of global cirrus cloud statistics using HIRS, *J. Climate*, 7, 1972–1986, doi:10.1175/1520-0442(1994)007<1972:FYOGCC>2.0.CO;2, 1994. 26887
- Yu, F., Luo, G., and Ma, X.: Regional and global modeling of aerosol optical properties with a size, composition, and mixing state resolved particle microphysics model, *Atmos. Chem. Phys.*, 12, 5719–5736, doi:10.5194/acp-12-5719-2012, 2012. 26898
- Yu, H., Kaufman, Y. J., Chin, M., Feingold, G., Remer, L. A., Anderson, T. L., Balkanski, Y., Bellouin, N., Boucher, O., Christopher, S., DeCola, P., Kahn, R., Koch, D., Loeb, N., Reddy, M. S., Schulz, M., Takemura, T., and Zhou, M.: A review of measurement-based assessments of the aerosol direct radiative effect and forcing, *Atmos. Chem. Phys.*, 6, 613–666, doi:10.5194/acp-6-613-2006, 2006. 26873
- Yu, T., Rose, W. I., and Prata, A. J.: Atmospheric correction for satellite-based volcanic ash mapping and retrievals using “split window” IR data from GOES and AVHRR, *J. Geophys. Res.*, 107, 4311, doi:10.1029/2001JD000706, 2002. 26874
- Yue, Q. and Liou, K.: Cirrus cloud optical and microphysical properties determined from AIRS infrared spectra, *Geophys. Res. Lett.*, 36, L05810, doi:10.1029/2008GL036502, 2009. 26878
- Zehner, C. (Ed.): Monitoring Volcanic Ash from Space, ESA-EUMETSAT workshop on the 14 April to 23 May 2010 eruption at the Eyjafjöll volcano, South Iceland, STM-280, ESA, Noordwijk, The Netherlands, doi:10.5270/atmch-10-01, 2012. 26895

5 Zhang, Q., Jimenez, J. L., Canagaratna, M. R., Allan, J. D., Coe, H., Ulbrich, I., Alfarra, M. R., Takami, A., Middlebrook, A. M., Sun, Y. L., Dzepina, K., Dunlea, E., Docherty, K., DeCarlo, P. F., Salcedo, D., Onasch, T., Jayne, J. T., Miyoshi, T., Shimojo, A., Hatakeyama, S., Takegawa, N., Kondo, Y., Schneider, J., Drewnick, F., Borrmann, S., Weimer, S., Demerjian, K., Williams, P., Bower, K., Bahreini, R., Cottrell, L., Griffin, R. J., Rautiainen, J., Sun, J. Y., Zhang, Y. M., and Worsnop, D. R.: Ubiquity and dominance of oxygenated species in organic aerosols in anthropogenically-influenced Northern Hemisphere midlatitudes, *Geophys. Res. Lett.*, 34, L13801, doi:10.1029/2007GL029979, 2007. 26898

**Aerosol type specification in the infrared**

L. Clarisse et al.

Title Page

Abstract

Introduction

Conclusions

References

Tables

Figures

⏪

⏩

◀

▶

Back

Close

Full Screen / Esc

Printer-friendly Version

Interactive Discussion



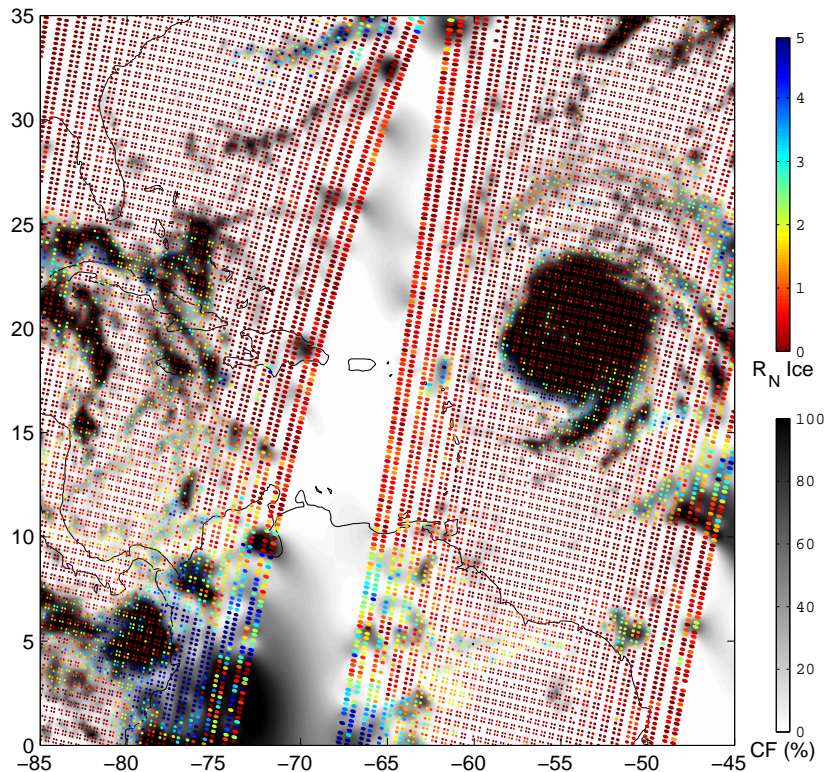


**Fig. 1.** IASI overpass on 15 September 2010. Shown in grays is the smoothed EUMETSAT Level 2 cloud fraction. The overlay scatter plot in color is the  $R_N$  for ice crystals as described in the text. Over the Atlantic Ocean is hurricane Igor, with cirrus clouds detected away from its center.

**Aerosol type specification in the infrared**

L. Clarisse et al.

Title Page

Abstract

Introduction

Conclusions

References

Tables

Figures

◀

▶

◀

▶

Back

Close

Full Screen / Esc

Printer-friendly Version

Interactive Discussion



Discussion Paper | Discussion Paper | Discussion Paper | Discussion Paper | Discussion Paper

## Aerosol type specification in the infrared

L. Clarisse et al.

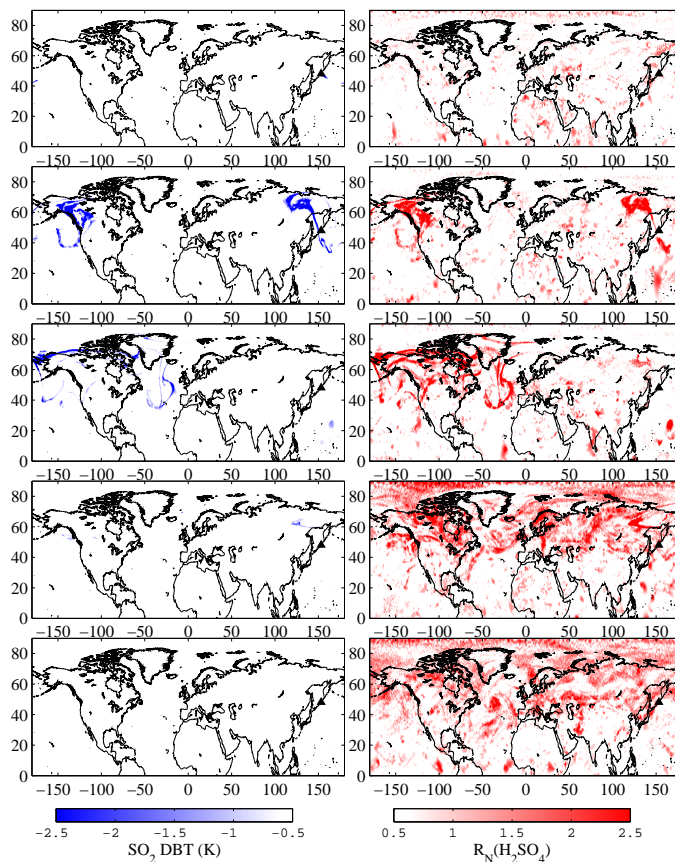


**Fig. 2.** View of the Northern Hemisphere on five different days (from top to bottom): 12 June (onset of the volcanic eruption of Sarychev), 19 June, 26 June, 12 July and 12 September 2009. On the left, the SO<sub>2</sub> BTD is shown and on the right  $R_N(\text{H}_2\text{SO}_4)$ .

## Aerosol type specification in the infrared

L. Clarisse et al.

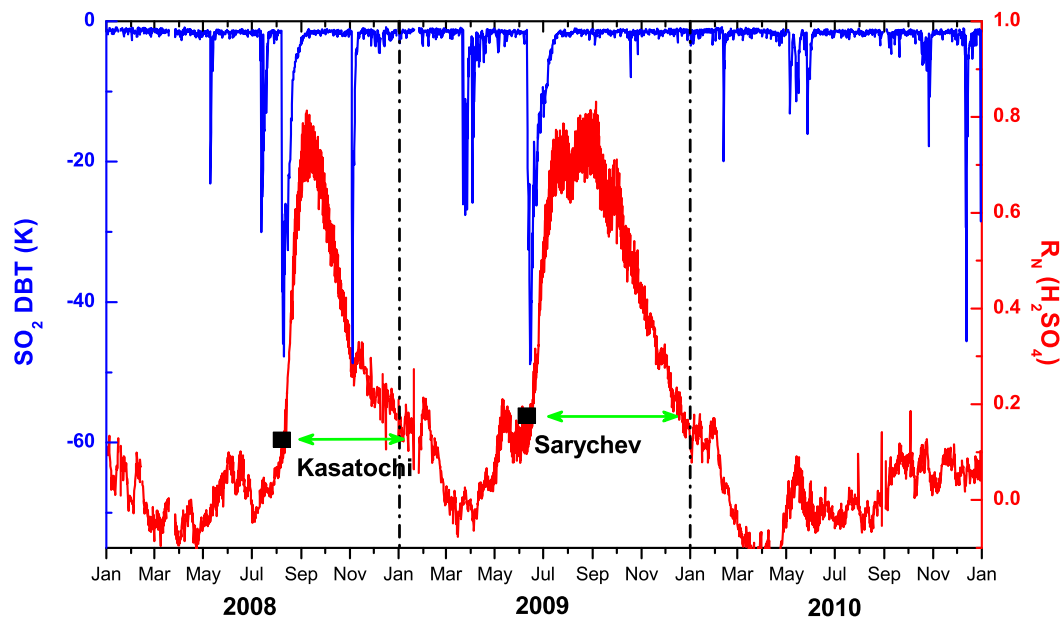


**Fig. 3.** Three years IASI timeseries of the Northern Hemisphere minimum daily value SO<sub>2</sub> DBT and the average daily value of  $R_N(\text{H}_2\text{SO}_4)$ .

Title Page

Abstract

Introduction

Conclusions

References

Tables

Figures

◀

▶

◀

▶

Back

Close

Full Screen / Esc

Printer-friendly Version

Interactive Discussion



**Aerosol type  
specification in the  
infrared**

L. Clarisse et al.

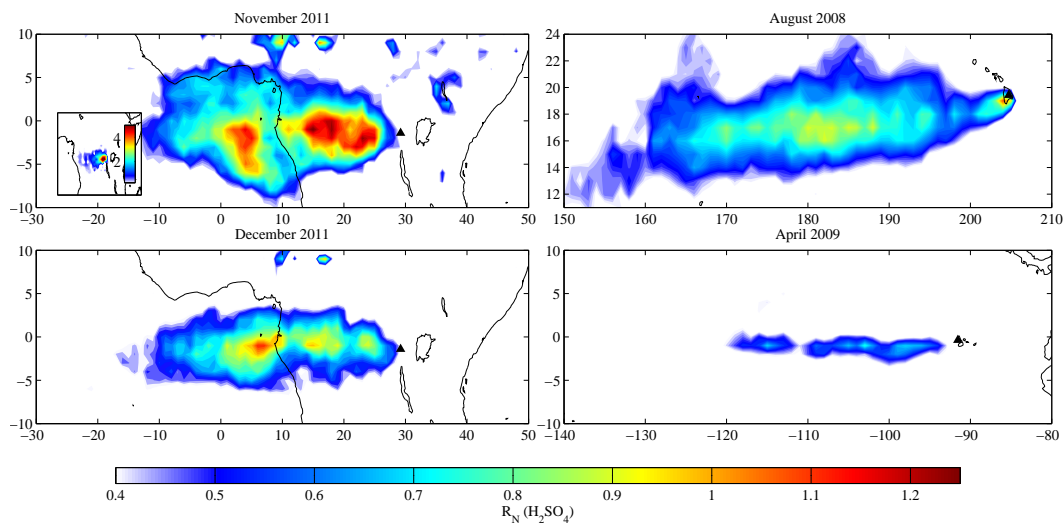


**Fig. 4.** Monthly averaged maps of  $R_N(\text{H}_2\text{SO}_4)$  for selected months and locations. The left panel shows plumes from Nyamuragira (D.R. Congo) in November (top) and December 2011. The inset in the top left panel shows the corresponding OMI  $\text{SO}_2$  average in DU (figure courtesy N. Theys, see Theys et al., 2012). Top right depicts the plume from Kilauea (Hawaii) for August 2008, bottom right from Fernandina (Galápagos Islands) for April 2009.

Title Page

Abstract

Introduction

Conclusions

References

Tables

Figures

◀

▶

◀

▶

Back

Close

Full Screen / Esc

Printer-friendly Version

Interactive Discussion



## Aerosol type specification in the infrared

L. Clarisse et al.

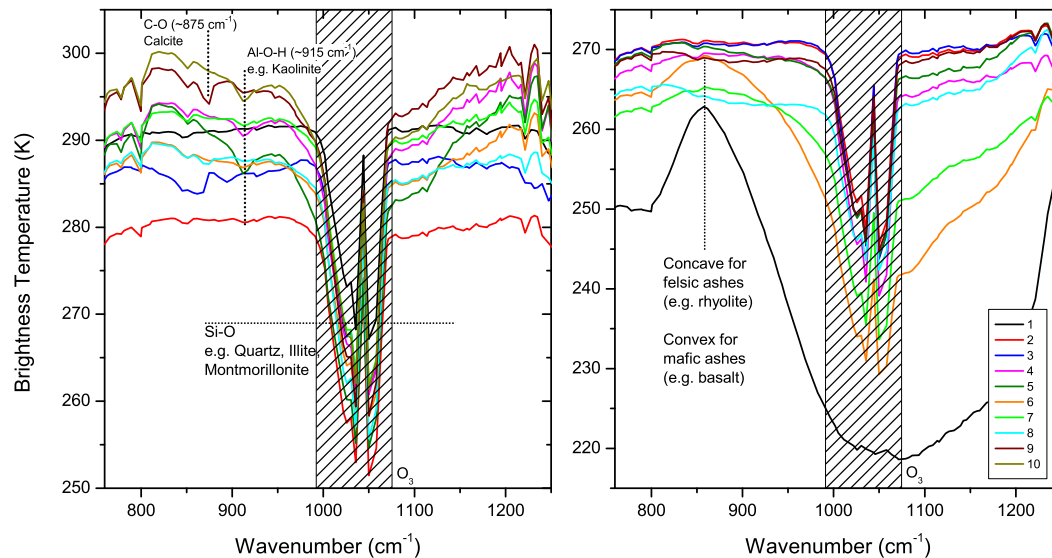


**Fig. 5.** Clustered mean spectra for sand (left panel) and volcanic ash (right panel) as generated by the *k*-means algorithm on spectra observed over a variety of airborne sand and ash plumes, respectively. The broadband V-shape absorption between 800–1200  $\text{cm}^{-1}$  due to Si-O is seen in most spectra. Some other mineral features are depicted in as well.

Title Page

Abstract

Introduction

Conclusions

References

Tables

Figures

◀

▶

◀

▶

Back

Close

Full Screen / Esc

Printer-friendly Version

Interactive Discussion

## Aerosol type specification in the infrared

L. Clarisse et al.

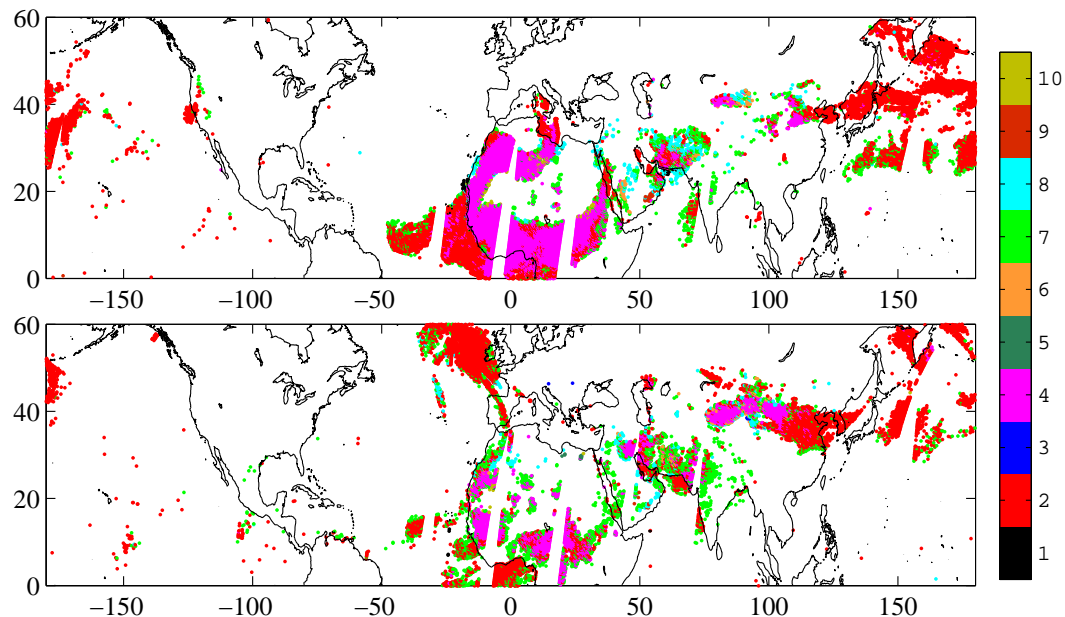


**Fig. 6.** Sand aerosols detected over the Northern Hemisphere on 23 March 2010 (top) and 8 April 2011 (bottom) based on strict thresholds for  $R_N$  and  $A_N$  for each of the ten tests. The colorcode corresponds to the test which passed (see Fig. 5). In case multiple tests flagged an observation, only the lowest test number is indicated.

[Title Page](#)[Abstract](#)[Introduction](#)[Conclusions](#)[References](#)[Tables](#)[Figures](#)[◀](#)[▶](#)[◀](#)[▶](#)[Back](#)[Close](#)[Full Screen / Esc](#)[Printer-friendly Version](#)[Interactive Discussion](#)

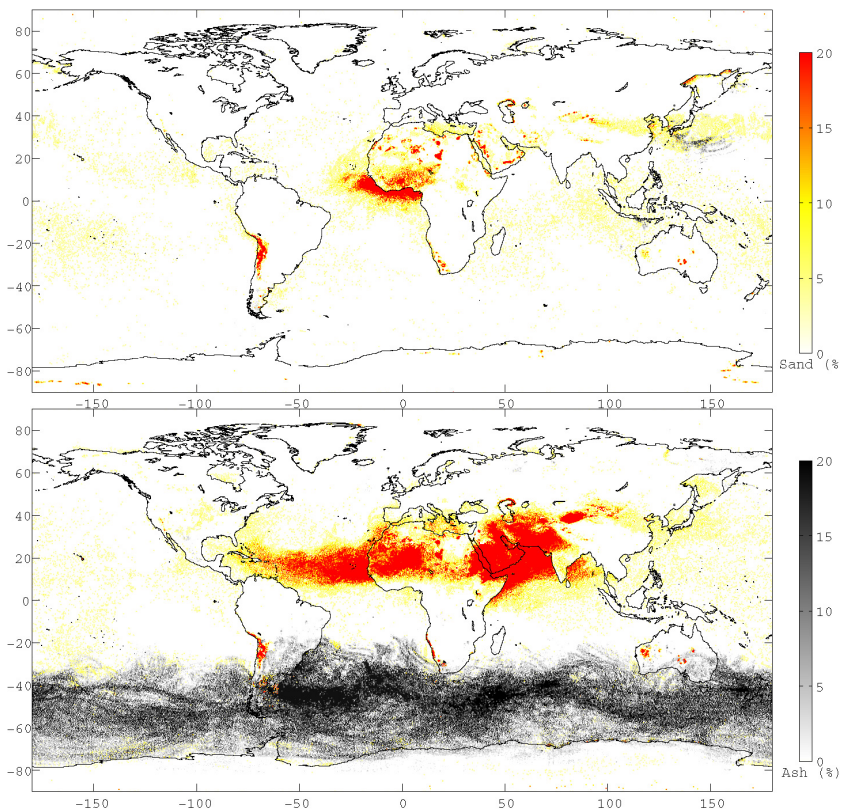


**Fig. 7.** Ash and sand detection in January (top panel) and June (bottom panel) 2011 in percentages per grid cell. In case both sand and ash were detected in the same grid cell all observations were assigned to one category based on the relative number count: when the number of sand detections was lower than twice the number of ash detections it was marked as ash, otherwise as sand.

**Aerosol type specification in the infrared**

L. Clarisse et al.

Title Page

Abstract Introduction

Conclusions References

Tables Figures

◀ ▶

◀ ▶

Back Close

Full Screen / Esc

Printer-friendly Version

Interactive Discussion



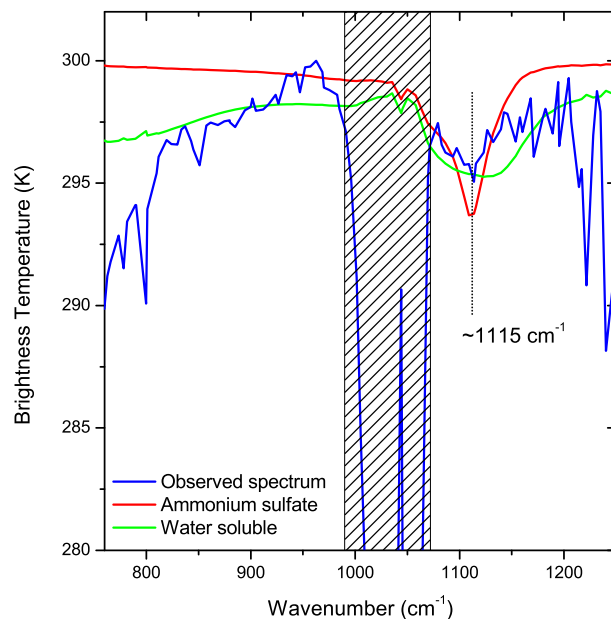


**Fig. 8.** Ammonium sulfate signatures in observed and simulated spectra. The blue spectrum was observed over East China in June 2010. Simulated spectra are shown using two different sets of refractive indices. The red spectrum uses refractive indices of crystalline ammonium sulfate from Earle et al. (2006), and reproduces the absorption feature around  $1115\text{ cm}^{-1}$  well. The green spectrum uses refractive indices of water soluble aerosol (Volz, 1972a,b; Shettle and Fenn, 1979) containing 80 %  $\text{H}_2\text{O}$  (Hess et al., 1998). It has a large ammonium sulfate component but also other components which reproduce to some extent the observed slope between  $800$  and  $1000\text{ cm}^{-1}$ .

**Aerosol type specification in the infrared**

L. Clarisse et al.

Title Page

Abstract

Introduction

Conclusions

References

Tables

Figures

◀

▶

◀

▶

Back

Close

Full Screen / Esc

Printer-friendly Version

Interactive Discussion



## Aerosol type specification in the infrared

L. Clarisse et al.

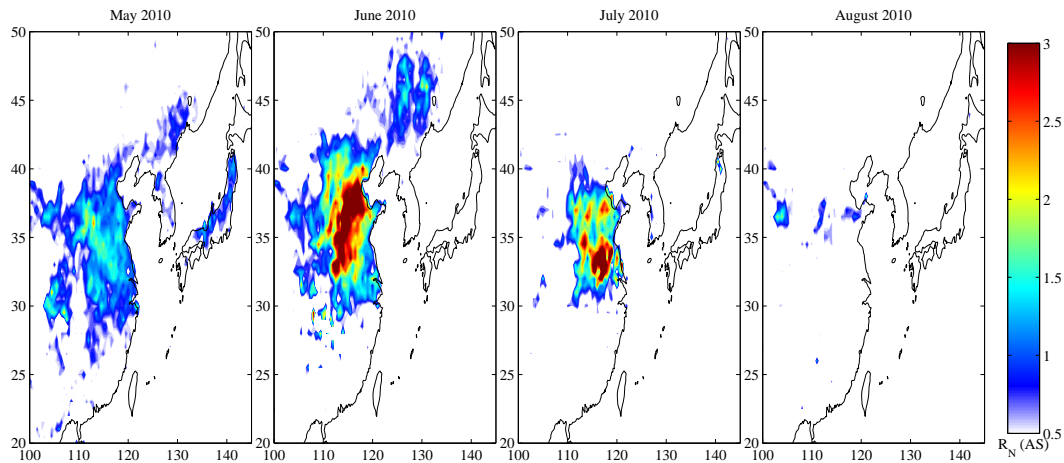


**Fig. 9.** Ammonium sulfate detected over East China for four consecutive months May–August 2010 (land only).

[Title Page](#)[Abstract](#)[Introduction](#)[Conclusions](#)[References](#)[Tables](#)[Figures](#)[◀](#)[▶](#)[◀](#)[▶](#)[Back](#)[Close](#)[Full Screen / Esc](#)[Printer-friendly Version](#)[Interactive Discussion](#)

## Aerosol type specification in the infrared

L. Clarisse et al.

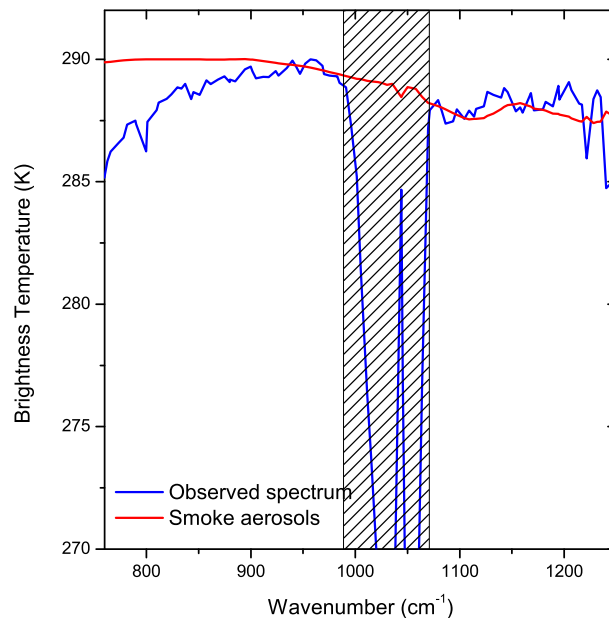


**Fig. 10.** Smoke aerosol signatures in observed and simulated spectra. The blue spectrum was observed over the Indian Ocean in October 2010. The red spectrum is a simulated spectrum using refractive indices of smoke from a mixed weed sample (Sutherland and Khanna, 1991).

[Title Page](#)[Abstract](#)[Introduction](#)[Conclusions](#)[References](#)[Tables](#)[Figures](#)[◀](#)[▶](#)[◀](#)[▶](#)[Back](#)[Close](#)[Full Screen / Esc](#)[Printer-friendly Version](#)[Interactive Discussion](#)

## Aerosol type specification in the infrared

L. Clarisse et al.

Title Page

Abstract

Introduction

Conclusions

References

Tables

Figures

◀

▶

◀

▶

Back

Close

Full Screen / Esc

Printer-friendly Version

Interactive Discussion

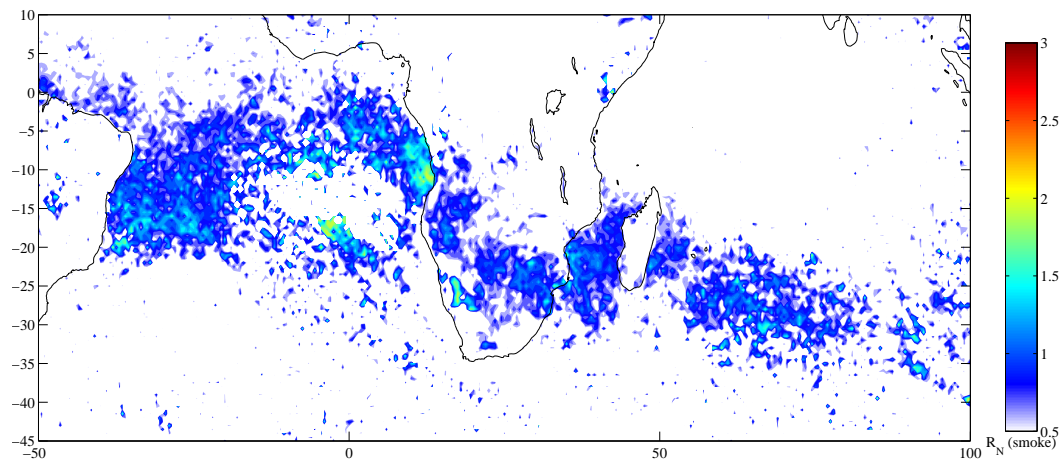


**Fig. 11.** October 2010 mean value of  $R_N$  for smoke over the South Atlantic and Indian Ocean.